NASA TECHNICAL NOTE

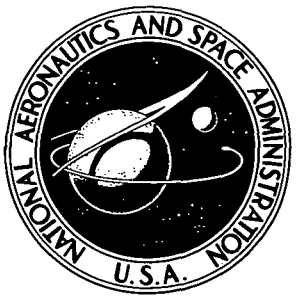

NASA TN D-7197

NASA TN D-7197

A METHOD FOR PREDICTING SHOCK SHAPES AND PRESSURE DISTRIBUTIONS ON TWO-DIMENSIONAL AIRFOILS AT LARGE ANGLES OF ATTACK

by George E. Kaattari

Ames Research Center
Moffett Field, Calif. 94035

NATIONAL AERONAUTICS AND SPACE ADMINISTRATION • WASHINGTON, D. C. • MARCH 1973

1. Report No.	2. Government Accession No.	3. Recipient's Catalog No.
NASA TN D-7197		

4. Title and Subtitle	5. Report Date
A METHOD FOR PREDICTING SHOCK SHAPES AND PRESSURE DISTRIBUTIONS ON TWO-DIMENSIONAL AIRFOILS AT LARGE ANGLES OF ATTACK	March 1973
	6. Performing Organization Code

7. Author(s)	8. Performing Organization Report No.
George E. Kaattari	A-4564
	10. Work Unit No.
9. Performing Organization Name and Address	117-07-02-01-00-21
NASA Ames Research Center Moffett Field, Calif. 94035	11. Contract or Grant No.
	13. Type of Report and Period Covered
12. Sponsoring Agency Name and Address	Technical Note
National Aeronautics and Space Administration Washington, D.C.	14. Sponsoring Agency Code

15. Supplementary Notes

16. Abstract

A method is presented for determining shock envelopes and pressure distributions for two-dimensional airfoils at angles of attack sufficiently large to cause shock detachment and subsonic flow over the windward surface of the airfoil. Correlation functions obtained from exact solutions are used to relate the shock standoff distance at the stagnation and sonic points of the body through a suitable choice for the shock shape. The necessary correlation functions were obtained from perfect gas solutions but may be extended to any gas flow for which the normal shock-density ratio can be specified.

17. Key Words (Suggested by Author(s))	18. Distribution Statement
Cones Pressure distributions Shock-layer thickness Wing-body	Unclassified - Unlimited

19. Security Classif. (of this report)	20. Security Classif. (of this page)	21. No. of Pages	22. Price*
Unclassified	Unclassified	50	$3.00

* For sale by the National Technical Information Service, Springfield, Virginia 22151

Page Intentionally Left Blank

NOTATION

a	semiminor axis of ellipse
B_b	body bluntness parameter for conic section ($(b/a)^2$ for ellipse) defined by $y^2 = 2R_b x - B_b x^2$ (ref. 1)
B_s	shock bluntness parameter for conic section defined by $y^2 = 2R_s x - B_s x^2$ (ref. 1)
b	semimajor axis of ellipse or span measured from shock apex
C	constant in stream function (eq. (C1))
c	chord or body length
$\bar{c}$	length along chord normalized by c
f	scale factor (eqs. (D7), (D8))
G	stagnation point mass-flow function (eq. (3))
k_0, k_1	constants in velocity distribution functions (eqs. (39)-(42))
M	Mach number
m-m	location of control surface (sketches (e) and (f))
n	correlation exponent (eq. (15))
P	pressure on body
$\mathcal{R}$	streamline radius behind shock
R_b	wing section or body radius at stagnation point
R_s	shock radius at apex
r	edge or corner radius
r_m	base radius of conical body (fig. 15)
r^t	body radius of section between tangent points (sketch (j))
s	distance on body surface from stagnation point
$\bar{s}$	distance from stagnation point normalized by s^*
u	velocity component in ξ,η coordinate system (sketch (h))
V	velocity

$\bar{V}$	local stream velocity normalized by V^*
$\dot{\bar{V}}$	derivative of $\bar{V}$ with respect to $\bar{s}$
ΔV	correction term to velocity distribution function (table 2)
v	velocity component in ξ,η coordinate system (sketch (h))
$\bar{v}$	dimensionless Newtonian velocity
$\Delta\bar{v}',\Delta\bar{v}''$	nonlinear components of $\bar{v}$ (sketch (d))
$\bar{v}_B$	base (linear) component of $\bar{v}$ (sketch (d))
$\dot{\bar{v}}$	derivative of $\bar{v}$ with respect to $\bar{s}$
X,Y	coordinate system defined in figure 10
X_s,Y_s	shock apex coordinates, figure 10
x,y	coordinate system with origin at shock apex
Y_m	reference ordinate, figure 10
y_s	vertical distance at shock between shock apex and stagnation streamline (sketches (b) and (i))
y_{st}	vertical distance at body between shock apex and stagnation point (sketches (b) and (i))
y^*	vertical distance between shock apex and sonic point on body (sketch (a))
α	angle of attack
γ	specific heat ratio
Δ	shock standoff distance
δ	stream deflection angle behind shock
ϵ	angle of tangency point of edge radius with respect to chord plane normal (sketch (c))
ζ	vorticity
θ	shock surface inclination with respect to plane normal to free-stream direction; in degrees, except where defined otherwise
ξ,η	coordinate system with origin of stagnation point (sketch (h))
ρ	gas density

ρ_θ	density of gas behind shock inclined at angle θ
$\overline{\rho V}$	average mass flow per unit area passing a specified control surface
ϕ	body surface inclination with respect to plane normal to free-stream direction; in degrees, except where noted
ψ	stream function (eq. (C1))
Ω	stagnation stream impingement angle (sketch (h))
∇	correction term to trial shock apex location

Subscripts

c	cylinder
ℓ	lower
n	normal to control surface
p	plate
$\mathscr{R}$	at shock location where streamline has the radius of $\mathscr{R}$
st	at stagnation point or along stagnation streamline
u	upper
0	at location on body in free stream in direction from shock apex
1	free stream
2	behind normal shock

Superscripts

*	at sonic point location
t,t',t"	tangent point location on body (sketch (j))

A METHOD FOR PREDICTING SHOCK SHAPES AND PRESSURE DISTRIBUTIONS ON TWO-DIMENSIONAL AIRFOILS AT LARGE ANGLES OF ATTACK

George E. Kaattari

Ames Research Center

SUMMARY

A method is presented for determining shock envelopes and pressure distributions for two-dimensional airfoils at angles of attack sufficiently large to cause shock detachment and subsonic flow over the windward surface of the airfoil. Correlation functions obtained from exact solutions are used to relate the shock standoff distance at the stagnation and sonic points of the body through a suitable choice for the shock shape. The necessary correlation functions were obtained from perfect gas solutions but may be extended to any gas flow for which the normal shock-density ratio can be specified.

INTRODUCTION

There is current interest in the aerodynamics of planetary atmospheric entry vehicles. Such vehicles are blunted to ensure a detached shock envelope in order to minimize vehicle heating rates during the flight trajectory.

Most theoretical and experimental investigations have been devoted to the prediction and measurement of shock envelopes and pressure distributions about axisymmetric shapes. Some attention has also been given to a limited class of two-dimensional cylindrical bodies (ref. 1) and to two-dimensional asymmetric flow about flat plates at large angles of attack (ref. 2). However, solutions for asymmetric two-dimensional shapes are not readily available.

This investigation was undertaken to develop an approximate method for estimating the shock envelope and pressure distribution over the windward surface of a large variety of two-dimensional profiles at angles of attack sufficiently large to result in shock detachment. The method employs a technique similar to that described in reference 3 but utilizes correlations based on available exact solutions for two-dimensional flows.

ANALYSIS

The analysis will be developed in four parts. First, the effect of body shape on the velocity gradients and shock standoff distance along the stagnation streamline is considered. Second, basic relationships between shock and body geometry in symmetric flow are derived and applied to symmetric flow shock solutions. Third, the symmetric flow relationships are modified and extended

to asymmetric flow shock solutions and demonstrated with a numerical example. Finally, the method for estimating the pressure distribution is developed and demonstrated by a numerical example.

Computing forms and necessary figures are provided to organize and expedite both the shock and pressure distribution calculations.

Stagnation Point Velocity Gradients

The effect of body radius on the velocity gradients and the shock standoff distance along the stagnation streamline is established as follows: Traugott (ref. 4) showed that the dimensionless velocity gradient at the stagnation point on a blunt body is a function only of the free-stream flow properties, M_1 and γ:

$$\frac{\Delta_{st}}{V_1}\frac{(dV/ds)_{st}}{(1 + \Delta_{st}/R_b)} = f(M_1,\gamma) \tag{1}$$

Assuming that this correlation is applicable to all shock solutions, any particular solution can be used to determine $f(M_1,\gamma)$. Accordingly, the solutions in reference 1 for shock-standoff distances, Δ_{st}/R_b, and pressure distributions on circular cylinders were used to extract numerical values for the velocity gradient in the vicinity of the stagnation point for various specific-heat ratios, γ, and free-stream Mach numbers. Substituting this gradient into equation (1), which can be rearranged into a convenient form, yields numerical values for $f(M_1,\gamma)$:

$$f(M_1,\gamma) = \frac{\frac{\Delta_{st}}{R_b}\frac{R_b}{V_1}\left(\frac{dV}{ds}\right)_{st}}{\left(1 + \frac{\Delta_{st}}{R_b}\right)} \tag{2}$$

For purposes of the flow continuity analysis described in appendix A, equation (2) is modified to obtain the stagnation point mass-flow gradient:

$$\frac{1}{(1 + \Delta_{st}/R_b)}\left[\frac{d(\rho_{st}V/\rho_1V_1)}{d(s/\Delta_{st})}\right]_{st} = \frac{\rho_{st}}{\rho_1} f(M_1,\gamma) \equiv G \tag{3}$$

The function G is plotted as a function of the normal shock-density ratio, ρ_2/ρ_1, (rather than Mach number) in figure 1. A close empirical fit to the curves is given by

$$G = \frac{3(\gamma+1)}{10} + \left[\frac{9}{4} - \frac{5}{3}(\gamma-1)\right]\frac{\rho_1}{\rho_{st}} \tag{4}$$

where

$$\frac{\rho_1}{\rho_{st}} = \frac{\rho_1}{\rho_2}\left[1 - \frac{\gamma-1}{\gamma+1}\frac{\rho_1}{\rho_2}\right]^{\frac{1}{\gamma-1}}$$

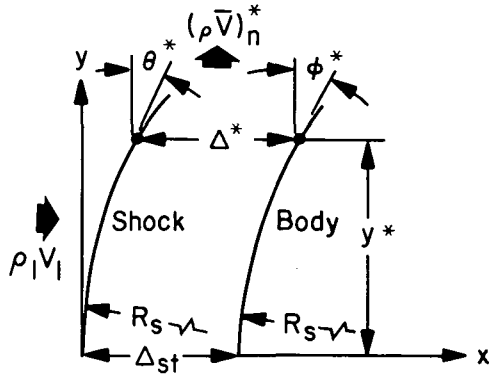

Sketch (a)

Symmetrical Shock Solutions

The shock solution is based on flow continuity considerations applied to the region between the body and its associated shock depicted in sketch (a). The length Δ_{st} represents the shock standoff distance from the body in the symmetry plane and, for a given free-stream flow, is related to the body and shock radii, R_b and R_s, as will be shown.

The length Δ^* represents the shock standoff distance from the sonic point on the body located at y^*. The ratio Δ^*/y^* depends on the sonic point inclination angle, ϕ^*, for a given free-stream flow. This dependence establishes a unique relationship between ϕ^* and the shock inclination angle, θ^*, as will be shown.

As a consequence of the foregoing, if ϕ^* and y^* can be specified for a body in a given flow, the parameters Δ_{st}, R_s, Δ^*, and θ^* are determined and constitute the shock solution. For this purpose, explicit relationships between the shock and body parameters are developed in the following sections.

Shock shape—Reference 1 defined shock traces as conic sections of suitable bluntness B_s (see Notation) and obtained the shock solutions for a range of conic-section blunt bodies. In the present investigation, it was assumed that conic sections can closely approximate the shock trace for a larger variety of blunt bodies than were considered in reference 1. The shock bluntness, B_s, is determined from the shock parameters R_s, y^*, and θ^* by

$$B_s = \left(\frac{R_s}{y^*}\right)^2 - \frac{1}{\tan^2\theta^*} \tag{5}$$

Shock and body parameters at symmetry plane—A mass-flow continuity analysis applied to a "volume" element adjacent to the plane of symmetry in two-dimensional flow results in the following relationship for the shock and body radii, R_s and R_b, the shock standoff distance, Δ_{st}, and the normal shock-density ratio:

$$\left(2 + \frac{\Delta_{st}}{R_b}\right) - \left(1 + \frac{\Delta_{st}}{R_b}\right)\left(1 - \frac{\Delta_{st}}{6R_b}\right) G$$

$$= \left(1 + \frac{2\Delta_{st}}{3R_b}\right)\left(\frac{\rho_2}{\rho_1} - 1\right)\frac{\Delta_{st}}{R_s} - \frac{1}{2}\left(1 + \frac{\Delta_{st}}{R_b}\right)\left[\frac{1}{3}\left(\frac{\rho_2}{\rho_1}\right)^2 - \frac{\gamma+3}{\gamma+1}\left(\frac{\rho_2}{\rho_1}\right) + \frac{2}{3}\right]\left(\frac{\Delta_{st}}{R_s}\right)^2 \tag{6}$$

A detailed derivation of equation (6) is presented in appendix A. The values of Δ_{st}/R_s as a function of Δ_{st}/R_b for various ratios ρ_2/ρ_1 are presented in figure 2.

Shock and body parameters at sonic "plane"—The average mass-flow component normal to the control surface Δ^* (sketch (a)) is denoted as $(\overline{\rho V})^*_n$. Mass-flow continuity fixes the ratio Δ^*/y^* as follows:

$$\frac{\Delta^*}{y^*} = \frac{\rho_1 V_1}{(\overline{\rho V})^*_n} \tag{7}$$

The mean normal mass-flow component, $(\overline{\rho V})^*_n$, was determined as follows: The value, ρV, has the maximum value of

$$\rho^* V^* = \rho_1 V_1 (\rho_2/\rho_1)^{1/2} \{2/[(\gamma+1) - (\gamma-1)(\rho_1/\rho_2)]\}^{1/\gamma-1}$$

at the sonic point and its derivative taken in any direction is zero. It was assumed that the second derivative at the sonic point is also zero. The normal (vertical) components of ρV at the shock and the body are, respectively, $\rho_1 V_1[(\rho_\theta/\rho_1)-1]\sin\theta^* \cos\theta^*$ and $\rho^* V^* \cos\phi^*$. These specifications on ρV are accommodated by a four-term polynomial in x/Δ^* which is integrated to obtain the normalized mean mass-flow value:

$$\int_0^1 \frac{\rho V}{\rho_1 V_1} \, d\left(\frac{x}{\Delta^*}\right) = \frac{(\overline{\rho V})^*_n}{\rho_1 V_1} = \frac{\left(\frac{\rho_\theta}{\rho_1} - 1\right)\sin\theta^* \cos\theta^* + 3\left(\frac{\rho^* V^*}{\rho_1 V_1}\right)\cos\phi^*}{4} = \frac{1}{(\Delta^*/y^*)} \tag{8}$$

Equation (8) indicates that, while primarily sensitive to the sonic angle ϕ^*, the value for Δ^*/y^* is determinate only if a functional relationship exists between the sonic angle ϕ^* and the shock angle θ^*. This functional relationship is established by shock solutions for a family of widely varying body shapes, including a flat plate, a circularly rounded slab, and a circular cylinder. The shock solutions for a flat plate and circularly blunted slabs are discussed in the following sections. These solutions, along with the circular cylinder solutions of reference 1, were then utilized to establish Δ^*/y^* and θ^* as functions of ϕ^*.

Flat plate—In the case of a flat plate supporting a shock of bluntness B_s, the sonic point is assumed to reside on the windward side of the plate corner, whence $\phi^* = 0$. Simple relationships between B_s, Δ_{st}/R_s, Δ^*/y^*, and θ^*_p with $\phi^* = 0$ were proposed in reference 3 for an axisymmetric disc on purely geometric grounds. These relationships also extend to two-dimensional flat plates and can be expressed in the present notation as follows:

$$B_s = R_s/\Delta_{st} \tag{9a}$$

$$(\Delta^*/y^*)_p = (\Delta_{st}/R_s)/\tan\theta^*_p \tag{9b}$$

Equations (8) and (9b) are combined to give

$$\frac{\Delta_{st}}{R_s} = \frac{4 \tan \theta_p^*}{\left(\frac{\rho_\theta}{\rho_1} - 1\right) \sin \theta_p^* \cos \theta_p^* + 3 \frac{\rho^* V^*}{\rho_1 V_1}} \tag{10}$$

Since Δ_{st}/R_s is known from equation (6) and since $\Delta_{st}/R_b = 0$, solutions for θ_p^* (eq. (10)) and for $(\Delta^*/y^*)_p$ (eq. (9b)) may be calculated for a flat plate. The results of such calculations are presented in figure 3 for $(\Delta^*/y^*)_p$ and in figure 4 for θ_p^* as functions of the normal shock-density ratio, ρ_2/ρ_1; the specific heat ratio, γ, is used as a parameter.

The equation for a shock with bluntness B_s can be expressed as

$$\frac{y^*}{R_s} = \frac{\tan \theta^*}{\sqrt{B_s \tan^2 \theta^* + 1}} \tag{11}$$

In the case of a flat plate, $y^* = b$ and $\theta^* = \theta_p^*$. Equations (9a) and (11) are combined to relate the centerline shock standoff distance, Δ_{st}, to the plate semiwidth, b:

$$\frac{\Delta_{st}}{b} = \frac{\sqrt{B_s \tan^2 \theta_p^* + 1}}{B_s \tan \theta_p^*} \tag{12}$$

The shock solution for a flat plate is now completely specified since B_s, Δ_{st}/b, $(\Delta^*/y^*)_p$, and θ_p^* are in hand.

Circularly blunted slab—It is assumed that a circularly blunted slab can be specified so that at some free-stream Mach number, a circular shock having nearly the same radius as that of the body will result. In this circumstance, $\Delta^* = \Delta_{st}$ and $\theta^* = \phi^*$, and with $y^* = R_s \sin \theta^* = R_b \sin \theta^*$, equation (8) gives

$$\frac{\Delta_{st}}{R_s} = \frac{4 \tan \theta^*}{\left(\frac{\rho_\theta}{\rho_1} - 1\right) \sin \theta^* + 3 \frac{\rho^* V^*}{\rho_1 V_1}} \tag{13}$$

The expression $\Delta_{st}/R_s = \Delta_{st}/R_b$ is determined using equation (6) and has a unique value for a given free-stream flow. Thus, $\theta^* = \phi^*$ is readily determined using equation (13) and the corresponding value of Δ^*/y^* is given by

$$\frac{\Delta^*}{y^*} = \frac{\Delta_{st}}{R_s \sin \theta^*} \tag{14}$$

Sonic angle, ϕ^*—In the foregoing, the shock solutions for a flat plate and a circularly blunted slab were determined once ϕ^* was fixed, that is, with $\phi^* = 0$ and with $\phi^* = \theta^*$. Shock solutions for other body shapes require general rules for selecting the appropriate sonic-point angle. The rules for

determining the sonic-point location and inclination angle follow those of reference 3. The arguments and pertinent equations are presented in appendix B. The essential results are given in figures 5 and 6. Figure 5 gives the reference sonic-point angle, ϕ_c^*, on a circular cylinder as a function of the reciprocal shock-density ratio, ρ_1/ρ_2, using the specific heat ratio, γ, as a parameter. Figure 6 gives the sonic-point angle ratio in the form $\sin \phi^*/\sin \phi_c^*$, either as a function of the body ellipticity ratio a/b or as a function of the ratio r/b (for a round-corner slab section).

Relationship of Δ^*/y^* and θ^* to ϕ^*—A preliminary plot of the calculated Δ^*/y^* values with $\sin \phi^*$ for a flat plate, a circularly blunted slab, and for a circular cylinder determined from reference 1 suggested a uniform exponential increase of Δ^*/y^* with $\sin \phi^*$. Accordingly, the three available Δ^*/y^* values were utilized to correlate Δ^*/y^* with $\sin \phi^*$ over the range, $0 < \phi^* < \phi_c^*$:

$$\frac{\Delta^*}{y^*} - \left(\frac{\Delta^*}{y^*}\right)_p = \left[\left(\frac{\Delta^*}{y^*}\right)_c - \left(\frac{\Delta^*}{y^*}\right)_p\right]\left(\frac{\sin \phi^*}{\sin \phi_c^*}\right)^n \tag{15}$$

The values $(\Delta^*/y^*)_c$ and $(\Delta^*/y^*)_p$ correspond to the circular cylinder and flat plate, respectively. The value of $\sin \phi^*$ is normalized by the circular cylinder value, $\sin \phi_c^*$. The value n was determined by substituting the values of Δ^*/y^* and ϕ^* from the circularly blunted slab solution into equation (15). The results of evaluating the expression $\Delta^*/y^* - (\Delta^*/y^*)_p$ as a function of $\sin \phi^*/\sin \phi_c^*$ are presented in figure 7 with the free-stream conditions expressed in terms of the normal shock-density ratio, ρ_2/ρ_1.

A preliminary plot of the three available θ^* values with $\sin \phi^*$ suggested a correlation curve of some complexity. Therefore, additional values of ϕ^* were required to define the relationship between θ^* and ϕ^*. Such values were calculated by utilizing the $\Delta^*/y^* - \phi^*$ relationship (fig. 7) with equation (8). The results are presented in figure 8, in which the term $\theta^* - \theta_p^*$ is expressed as a function of the normalized sonic-point angle variable, $\sin \phi^*/\sin \phi_c^*$, with normal shock-density ratio, ρ_2/ρ_1, as a parameter.

It is interesting that the correlations of Δ^*/y^* and θ^* with ϕ^* in the forms presented in figures 7 and 8 are independent of the specific heat ratio, γ. The application of these correlations to shock solutions in general will be demonstrated in a following section.

Asymmetrical Flow Shock Solutions

The pattern of asymmetrical shock is assumed to consist of an upper and a lower conic section of different bluntness, B_s; both sections, however, are assumed to have a common vertical tangent and radius of curvature, R_s, at the shock apex as shown in sketch (b). The appropriate sections constituting the shock are found by iterative calculations so that, ultimately, both upper and lower shock elements satisfy Δ^*/y^* values based on mass-flow continuity at

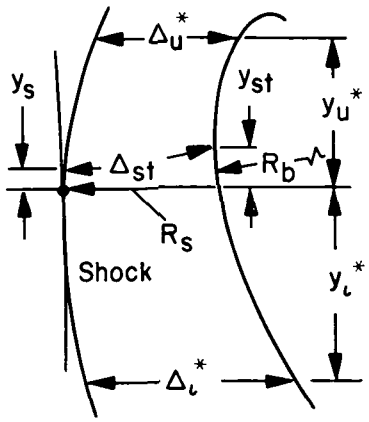

Sketch (b)

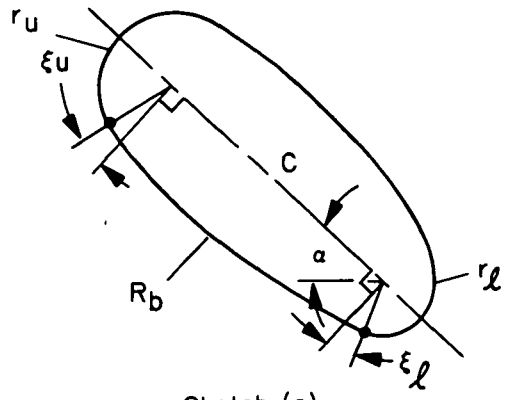

Sketch (c)

their respective body sonic-point ordinates. In this regard, it is assumed that equation (6) is applicable although the stagnation streamline is curved. The curvature of the stagnation streamline, however, does introduce certain stream displacements denoted by y_s and y_{st} in sketch (b). An approximate analysis of these displacements is presented in appendix C. The results of the analysis are presented in figure 9.

The asymmetrical solution is applied to a class of two-dimensional bodies typified by the section shown in sketch (c). The radii r_u and r_ℓ are the leading and trailing edge radii of the section whose chord length is c. These radii are tangent to a body arc of radius R_b. The tangency points fix the indicated angles, ε_u and ε_ℓ. The angle of attack, α, is measured between the chord and the free-stream direction.

The technique of the asymmetrical shock solution is best demonstrated by the following calculative example with necessary equations introduced as required.

Calculative example—The solution is applied to a wing-like body such as shown in sketch (c). The coordinate system most convenient to the solution is shown in figure 10 along with specific geometric details of the body in question.

The solution is based on an initially assumed value for the span b, which locates the shock apex (fig. 10). An approximate value for b is based on the following: If the angle of attack α is 90°, the flow will be nearly symmetrical and the shock apex will be located approximately at midchord, or, $b = c/2$. If the angle of attack is sufficiently small that a sonic point will reside at the point where r_u and R_b are tangent, the circular cylinder shock solution applies with $\phi_u^* = \phi_c^* = 90^0 - \alpha - \varepsilon_u$. The shock apex will then be located at $b = r_u$. A linear variation of b with an angle of attack α is assumed with the above limits, giving the following result:

$$\frac{b}{c} = \frac{1}{2} - \left[\frac{1}{2} - \frac{r_u}{c}\right]\left[\frac{90^\circ - \alpha}{\varepsilon_u + \phi_c^*}\right] \tag{16}$$

A trial shock solution can be calculated using the values $c = 1.0$, $r_u = 0.10$, $r_\ell = 0.05$, $R_b = 1.92$, $\varepsilon_u = 10°$, $\varepsilon_\ell = 16.5°$, and $\alpha = 65°$ (fig. 10).

A reference ordinate is defined as

$$Y_m = (c - r_u - r_\ell)\sin\alpha + r_u = (1.0 - 0.10 - 0.05)0.906 + 0.10 = 0.870 \tag{17}$$

The free-stream flow is ideal air at $M_1 = \infty$ ($\gamma = 1.4$, $\rho_2/\rho_1 = 6.0$). The basic shock parameters associated with the flow are as follows: $(\Delta^*/y^*)_p = 0.608$ (fig. 3); $\theta^*_p = 19.45°$ (fig. 4); and $\phi^*_c = 44.5°$ (fig. 5).

The approximate shock tangency point (apex), b, given by equation (16) can then be evaluated:

$$\frac{b}{c} = \frac{1}{2} - \left[\frac{1}{2} - \frac{0.10}{1.0}\right]\left[\frac{90° - 65°}{10° + 44.5°}\right] = 0.317$$

or

$$b = 0.317 \quad (c = 1.0)$$

The upper sonic angle, ϕ^*_u, is determined as follows: The ratio $r_u/b = 0.10/0.317 = 0.316$ takes the role of r/b in figure 6 where the ordinate value $\sin\phi^*/\sin\phi^*_c = 0.77$ is found. The value for $\phi^* = \sin^{-1}(0.77 \sin 44.5°) = 32.7°$ is calculated. This angle is compared with the inclination of the upper corner tangency point, $\phi^t_u = \alpha + \varepsilon - 90° = 65 + 10° - 90° = -15°$. The sonic-point angle criteria defined in appendix B require the larger of these angles to represent ϕ^*_u; therefore, $\phi^*_u = 32.7°$.

The upper sonic point coordinates are given by the following:

$$Y^*_u = Y_m - r_u(1 - \sin\phi^*_u) = 0.870 - 0.10(1 - 0.540) = 0.824 \tag{18}$$

$$X^*_u = (c - r_u - r_\ell)\cos\alpha + r_u\cos\phi^*_u = 0.85(0.422) + 0.10(0.842) = 0.443 \tag{19}$$

With the angle ϕ^*_u specified, the ratio $(\Delta^*/y^*)_u$ and the shock angle θ^* are determined as follows: The values $(\Delta^*/y^*) - (\Delta^*/y^*)_p$ and $\theta^* - \theta^*_p$, associated with $\phi^*_u = 32.7°$ (at $\rho_2/\rho_1 = 6.0$), are found from figures 7 and 8 which give $(\Delta^*/y^*) - (\Delta^*/y^*)_p = 0.109$ and $\theta^* - \theta^*_p = -2.60°$, whence

$$(\Delta^*/y^*)_u = 0.109 + 0.608 = 0.717$$

and

$$\theta^*_u = -2.60° + 19.45° = 16.85°$$

The lower sonic angle, ϕ^*_ℓ, is determined as follows: The lower span, opposing the upper span b, has the value, $Y_m + r_\ell - b = 0.870 + 0.05 - 0.317 = 0.603$. The ratio, $r_\ell/(Y_m + r_\ell - b) = 0.05/0.603 = 0.083$, takes the role of r/b in

figure 6 where the ordinate, $\sin \phi^*/\sin \phi_c^* = 0.52$, is found. The value for $\phi_\ell^* = \sin^{-1}(0.52 \sin 44.5°) = 21.4°$ is calculated. This angle is compared with the inclination of the lower corner tangency point,

$$\phi_\ell^t = 90° + \varepsilon_\ell - \alpha = 90° + 16.5° - 65° = 41.5°$$

The previously mentioned sonic-angle criteria[1] requires the larger of these angles to represent ϕ^*; therefore, $\phi_\ell^* = 41.5°$.

The lower sonic-point coordinates are as follows:

$$Y_\ell^* = -r_\ell \sin \phi_\ell^* = -0.05(0.663) = -0.033 \tag{20}$$

$$X_\ell^* = r_\ell \cos \phi_\ell^* = 0.05(0.749) = 0.037 \tag{21}$$

The ratio $(\Delta^*/y^*)_\ell$ and the shock angle θ_ℓ^* will now be determined. The values $(\Delta^*/y^*) - (\Delta^*/y^*)_p$ and $\theta^* - \theta_p^*$, associated with $\phi^* = 41.5°$ $(\rho_2/\rho_1 = 6.0)$, can be determined from figures 7 and 8, which give $(\Delta^*/y^*) - (\Delta^*/y^*)_p = 0.165$ and $\theta^* - \theta_p^* = -1.30°$; therefore,

$$(\Delta^*/y^*)_\ell = 0.165 + 0.608 = 0.773$$

and

$$\theta_\ell^* = -1.30° + 19.45° = 18.15°$$

Sufficient information is now available to estimate the coordinates X_s and Y_s, of the shock "apex"

$$X_s = X_u^* + x_u^* + \Delta_u^* = X_u^* + y_u^*(x^*/y^*)_u + y_u^*(\Delta^*/y^*)_u \tag{22}$$

$$Y_s = Y_m - b \tag{23}$$

The value

$$y_u^* = b - (Y_m - Y_u^*) = 0.317 - (0.870 - 0.824) = 0.271 \tag{24}$$

is the vertical displacement between the upper sonic point on the body and the shock apex. The value x_u^* is the horizontal displacement on the shock from the apex to the point where the shock inclination is θ_u^*. The displacement ratio, $(x^*/y^*)_u$, is approximated by the "mean" shock slope, $\tan(\theta_u^*/2)$. Equations (22) and (23) can now be evaluated:

$$X_s = 0.443 + 0.271 \tan \frac{16.85°}{2} + (0.271)(0.717) = 0.677$$

$$Y_s = 0.870 - 0.317 = 0.553$$

---

[1]Occasionally, the selection rule may give an angle $\phi_\ell^* > \phi_c^*$, in which case ϕ_ℓ^* is assigned the value of ϕ_c^*. In this event, the location on the body where its surface inclination is ϕ_c^* fixes the lower sonic-point coordinates.

The approximate shock apex is located by the above coordinates on figure 10 and is denoted by the circular symbol.

Attention is now given to defining the stagnation streamline. For this purpose, the length Δ_0 in the free-stream direction between the shock apex and the body, the associated body surface inclination ϕ_0, and the radius R_b at the body terminus of Δ_0 are required. These values may be calculated with the geometry of simple analytic body sections but, in general, are most expeditiously scaled from an accurate drawing of the section. In this case, the measurements from figure 10 are $\Delta_0 = 0.277$ and $\phi_0 = 21°$; R_b has the given value of 1.92 units. A simplified stagnation streamline consisting of two straight lines of equal length, one drawn horizontally and one drawn at the inclination ϕ_0, respectively, are located as indicated by the dashed line elements in figure 10. While this approximation lacks the qualitative feature of the actual uniformly curved streamline, its length,

$$\Delta_{st} \approx \Delta_0(1 + \cos \phi_0)/2 = 0.277(1 + 0.934)/2 = 0.268 \tag{25}$$

is a good approximation to that of the actual stagnation streamline. The angle ϕ_{st} at the point of the stagnation streamline impingement on the body is (in degrees) as follows:

$$\phi_{st} \approx \phi_0 - 57.3 \frac{\Delta_0}{2} \frac{\sin \phi_0}{R} = 21° - 57.3(0.277/2)(0.357)/1.92 = 19.5° \tag{26}$$

The stagnation streamline value, $\Delta_{st}/R_b = 0.268/1.92 = 0.140$, and the corresponding value, $\Delta_{st}/R_s = 0.200$, is found from figure 2 with $\rho_2/\rho_1 = 6.0$. The value $\Delta_{st}/R_s = 0.200$ with $\rho_2/\rho_1 = 6.0$ gives the ordinate $y_s/\Delta_{st} \sin \phi_{st} = 0.18$ from figure 9. The vertical displacement y_s of the dividing (stagnation) streamline from the shock apex is evaluated as follows:

$$y_s = (y_s/\Delta_{st} \sin \phi_{st})\Delta_{st} \sin \phi_{st} = 0.18(0.268)\sin 19.5° = 0.016 \tag{27}$$

The effect of the displacement y_s is to reduce the mass flow intercepted by the upper shock and to increase the mass flow intercepted by the lower shock. These mass-flow continuity considerations then affect the values of Δ^* as follows:

$$\left.\begin{aligned} \Delta_u^* &= (y_u^* - y_s)(\Delta/y)_u^* \\ \Delta_\ell^* &= (y_\ell^* + y_s)(\Delta/y)_\ell^* \end{aligned}\right\} \tag{28}$$

With the value of $R_s = \Delta_{st}/(\Delta_{st}/R_s) = 0.268/0.200 = 1.340$, an improved determination of the ratio x^*/y^* is made with the conic-section relationship:

$$\left(\frac{x^*}{y^*}\right) = \frac{\tan \theta^*}{1 + (R_s/y^*)\tan \theta^*} \tag{29}$$

A check of the shock apex or tangency point location X_s as given by *both* the upper and lower shock geometry is then made. For this purpose, the values of y^*, $(x^*/y^*)_u$, and $(x^*/y^*)_\ell$ need to be established first:

$$y_\ell^* = Y_m - b - Y_\ell^* = 0.870 - 0.317 - (-0.033) = 0.586 \tag{30}$$

With equation (29):

$$\left(\frac{x^*}{y^*}\right)_u = \frac{\tan 16.85°}{1 + \frac{1.340}{0.271}\tan 16.85°} = 0.121$$

and

$$\left(\frac{x^*}{y^*}\right)_\ell = \frac{\tan 18.15°}{1 + \frac{1.340}{0.586}\tan 18.15°} = 0.187$$

The shock apex location X_s is given for the upper and lower shock by

$$\left.\begin{aligned} X_{su} &= X_u^* + (y_u^* - y_s)\left(\frac{\Delta^*}{y^*}\right)_u + y_u^*\left(\frac{x^*}{y^*}\right)_u \\ &= 0.443 + (0.271 - 0.016)0.717 + 0.271(0.121) = 0.659 \\ X_{s\ell} &= X_\ell^* + (y_\ell^* + y_s)\left(\frac{\Delta^*}{y^*}\right)_\ell + y_\ell^*\left(\frac{x^*}{y^*}\right)_\ell \\ &= 0.037 + (0.586 + 0.016)0.773 + 0.586(0.187) = 0.612 \end{aligned}\right\} \tag{31}$$

A discrepancy or mismatch of $X_{s\ell} - X_{su} = 0.612 - 0.659 = -0.047$ is indicated. Since the above values for X_s are primarily affected by y_u^* and y_ℓ^*, an incremental correction term, ∇, is applied to these values so that $X_{s\ell} = X_{su}$. Equations (31) are modified accordingly and equated:

$$X_u^* + (y_u^* + \nabla)\left(1 - \frac{y_s}{y_u^* + \nabla}\right)\left(\frac{\Delta^*}{y^*}\right)_u + (y_u^* + \nabla)\left(\frac{x^*}{y^*}\right)_u = X_\ell^* + (y_\ell^* - \nabla)\left(1 + \frac{y_s}{y_\ell^* - \nabla}\right)\left(\frac{\Delta^*}{y^*}\right)_\ell + (y_\ell^* - \nabla)\left(\frac{x^*}{y^*}\right)_\ell \tag{32}$$

Equation (32) is solved for ∇ (neglecting nonlinear terms in ∇) with the result

$$\nabla = \frac{X_{s\ell} - X_{su}}{\left(\frac{x^*}{y^*}\right)_u + \left(\frac{\Delta^*}{y^*}\right)_u + \left(\frac{x^*}{y^*}\right)_\ell + \left(\frac{\Delta^*}{y^*}\right)_\ell} = \frac{-0.047}{0.121 + 0.717 + 0.187 + 0.773} = -0.026 \tag{33}$$

The above correction, $\nabla = -0.026$, when applied to $b = 0.317$, automatically modifies the values, y_u^* and y_ℓ^*, to the required values.

An iterative calculation is then made with the modified value, $b = 0.317 - 0.026 = 0.291$, replacing the initial value, $b = 0.317$. The calculations are repeated with the exception that the initial value $(x^*/y^*)_u = \tan(\theta_u^*/2)$, used in equation (22), is replaced by the value $(x^*/y^*)_u$

from equation (29). This substitution is clarified by examining the computing form presented in table 1. This form contains the foregoing calculations and presents the numerical results of iterations toward a convergent solution. The final results include the ordinate of the stagnation point location Y_{st} on the body and the shock bluntness parameters B_{su} and $B_{s\ell}$ given by equation (5).

Pressure Distribution

The pressure distribution is found by first determining the velocity distribution $V/V^* = \bar{V}(\bar{s})$, where $\bar{s} = s/s^*$, and applying the perfect gas relationship

$$\frac{P}{P_{st}} = \left[1 - \frac{\gamma-1}{\gamma+1}\left(\frac{V}{V^*}\right)^2\right]^{\frac{\gamma}{\gamma-1}} \tag{34}$$

to give P/P_{st} as a function of $\bar{s}$. This application is expedited through figure 11 which gives P/P_{st} as a function of V/V^* for various values of the specific heat ratio, γ.

The method, in principle, is as follows: The velocity distribution function is first determined for what is considered an analytic (smooth) body approximating the actual body shape. A correction term is then added if necessary to account for the effect of surface curvature discontinuities. The desired function $\bar{V}(\bar{s})$ is subject to the constraints $\bar{V}(0) = 0$ and $\bar{V}(1) = 1$; the associated derivatives $\dot{\bar{V}}(0)$ and $\dot{\bar{V}}(1)$ are then evaluated at the stagnation and sonic points.

The value of the stagnation point derivative $\dot{\bar{V}}(0)$ is found by rearranging terms in equation (3) with $V_1/V^* = (\rho_2/\rho_1)^{1/2}$:

$$\dot{\bar{V}}(0) = \frac{d(V/V^*)}{d(s/s^*)} = \sqrt{\frac{\rho_2}{\rho_1}}\,\frac{\rho_1}{\rho_{st}}\,G\left(1 + \frac{\Delta_{st}}{R_b}\right)\frac{s^*}{\Delta_{st}} \tag{35}$$

The values Δ_{st}/R_b and s^*/Δ_{st} are provided by the previously determined shock solution for the body in question.

The sonic point velocity derivative is related to the sonic point pressure derivative by differentiating equation (34) with respect to s/s^* and evaluating the result at $V/V^* = 1$:

$$\frac{d(P/P_{st})}{d(s/s^*)} = -\frac{\gamma P^* d(V/V^*)}{P_{st}\, d(s/s^*)} \tag{36}$$

The sonic pressure derivative, to a good approximation, is $-s^*/r$ (ref. 3). Substituting this value for the left side of equation (36) gives the value of the sonic point velocity derivative as follows:

$$\dot{\bar{V}}(1) = \frac{d(V/V^*)}{d(s/s^*)} = \frac{P_{st} s^*}{\gamma P^* r} \tag{37}$$

The next subsection presents the derivation of velocity functions subject to the above constraints and applicable to smooth bodies (no surface curvature discontinuities). The following subsection presents an approximate method that accounts for the effect of surface curvature discontinuities.

Velocity distribution for a smooth body—In reference 5 it was pointed out that in the vicinity of a sharp sonic corner, the velocity in the present notation is

$$\bar{V}(\bar{s}) \approx 1 - \sqrt{1 - \bar{s}} \tag{38}$$

Equation (38) satisfies the requirements that $\bar{V}(0) = 0$ and $\bar{V}(1) = 1$, and gives $\dot{\bar{V}}(1) = \infty$ in agreement with equation (37) for a sharp sonic corner ($r = 0$). Equation (38) is generalized in a simple manner to accommodate $\dot{\bar{V}}(1) \neq \infty$, but to retain the property, $\bar{V}(0) = 0$ and $\bar{V}(1) = 1$:

$$\bar{V}(\bar{s}) = \frac{1 - \sqrt{1 - k_1 \bar{s}}}{1 - \sqrt{1 - k_1}} \tag{39}$$

The appropriate constant, k_1, is determined by differentiating equation (39) and equating the result at $\bar{s} = 1$ to $\dot{\bar{V}}(1)$ (eq. (37)):

$$k_1 = \frac{4\dot{\bar{V}}(1)[\dot{\bar{V}}(1) - 1]}{[1 - 2\dot{\bar{V}}(1)]^2} \tag{40}$$

Equation (39) with k_1 satisfies the condition $\bar{V}(0)$, $\bar{V}(1)$, and $\dot{\bar{V}}(1)$, but only in fortuitous cases gives the correct value for $\dot{\bar{V}}(0)$. An independent velocity function is required to satisfy the conditions $\bar{V}(0)$, $\bar{V}(1)$, and $\dot{\bar{V}}(0)$. A monotonically increasing function, $\bar{V}(\bar{s})$, similar to that of equation (39) is chosen

$$\bar{V}(\bar{s}) = \frac{\sqrt{1 - k_0(1 - \bar{s})} - \sqrt{1 - k_0}}{1 - \sqrt{1 - k_0}} \tag{41}$$

where

$$k_0 = \frac{4\dot{\bar{V}}(0)[\dot{\bar{V}}(0) - 1]}{[1 - 2\dot{\bar{V}}(0)]^2}$$

Equation (41) satisfies the "end" conditions $\bar{V}(0)$, $\dot{\bar{V}}(0)$, and $\bar{V}(1)$. All "end" conditions are satisfied by a linear interpolation between the values given by equations (39) and (41):

$$\bar{V}(\bar{s}) = \left\{\frac{\sqrt{1 - k_0(1 - \bar{s})} - \sqrt{1 - k_0}}{1 - \sqrt{1 - k_0}}\right\}(1 - \bar{s}) + \left\{\frac{1 - \sqrt{1 - k_1 \bar{s}}}{1 - \sqrt{1 - k_1}}\right\}\bar{s} \tag{42a}$$

In cases where $\dot{\bar{V}}(0) < 0.5$, equation (42a) will not satisfy both $\dot{\bar{V}}(0)$ and $\bar{V}(1) = 1$. A truncated series term is substituted for such cases:

$$\bar{V}(\bar{s}) = [\dot{\bar{V}}(0)\bar{s} + (1 - \dot{\bar{V}}(0))\bar{s}^2](1 - \bar{s}) + \left\{\frac{1 - \sqrt{1 - k_1\bar{s}}}{1 - \sqrt{1 - k_1}}\right\}\bar{s} \qquad (42b)$$

Equations (42a) and (42b) give a uniform velocity distribution and are presumably applicable to a smooth body of uniformly varying surface curvature.

Effect of curvature discontinuities—In cases where the location of the stagnation point is Newtonian (most forward point on the body) or when the absolute value of the body surface inclination angle increases with distance from the stagnation point, the effect of surface curvature discontinuities may be estimated in the following manner. Newtonian theory suggests the relationship $\bar{v} \approx \sin\phi$ (the lower case $\bar{v}$ is used to distinguish velocities from those given by equation (42)). The further approximation $\bar{v} \approx \phi$ (ϕ in radians), is adopted to simplify the analysis. The body surface is assumed to consist of three tangent radii, R_b, r^t, and r. The values of $\bar{v} = \phi$ associated with $\bar{s} = 0$, the tangent points, and at $\bar{s} = 1$ are, respectively, ϕ_{st}, $\phi^{t'}$, $\phi^{t''}$, and ϕ^* as shown in sketch (d). Straight-line elements are drawn between adjacent ϕ values resulting in a line function indicated by the solid line. The slopes of the individual elements are determined by the appropriate surface radius, that is, where the element radius is R_b, $\bar{V} = s^*/R_b$, etc. A smooth curve approximation to the line function is determined as follows: The midsection of the line function is extended to $\bar{s} = 0$ and $\bar{s} = 1$. The result is a linear base function, $\bar{v}_B$, to which smoothly varying incremental functions $\Delta\bar{v}'$ and $\Delta\bar{v}''$ of the form $\Delta\bar{v}' = C'(1-\bar{s})^{n'}$ and $\Delta\bar{v}'' = C''(\bar{s})^{n''}$ are added to match the line function ordinates and slopes at $\bar{s} = 0$ and $\bar{s} = 1$:

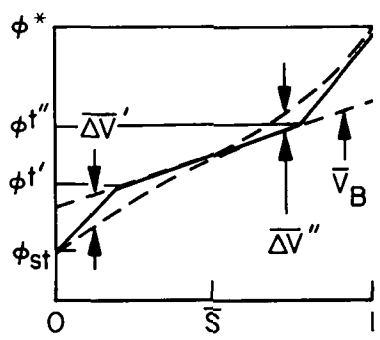

Sketch (d)

$$\bar{v} = \bar{v}_B - \Delta\bar{v}' + \Delta\bar{v}'' \qquad (43)$$

The smooth Newtonian velocity distribution, given by equation (43), is analogous to the velocity distribution given by equation (42). The difference in velocity distribution between the line function and equation (43) represents an additive correction term accounting for surface curvature discontinuities. It is assumed that this Newtonian correction, suitably scaled, can be applied to the distribution given by equation (42) to account for the effect of surface curvature discontinuities.

Detailed derivations giving the explicit form of equation (43) are omitted herein. Instead, the results of such derivations are embodied in the computing form presented in table 2. Additional instructions are given in appendix D.

Numerical example—In graphical form, figure 12 shows sample numerical results obtained with equation (42) for the velocity distribution on a smooth body equivalent to a blunted cone.[2] The appropriate velocity correction term

[2]While the shock solution presented herein applies only to two-dimensional flow, the method of determining the velocity distribution is general. The velocity gradients for this example (fig. 12) are determined from reference 3.

is provided by a calculated example in the computing form of table 2. Comments on the selection of suitable scaling factors and other details pertaining to the computing form are discussed in appendix D.

The pressure distribution corresponding to the corrected velocity distribution was determined from figure 11 and is included in figure 12.

COMPARISON OF EXPERIMENTAL AND PREDICTED RESULTS

The validity of the present method was assessed on the basis of comparisons with the theoretical shock envelopes of reference 2 and comparisons of pressure distributions with the theoretical results of references 1 and 5 and the experimental results of references 6 and 7.

Shock Shape

Comparisons of shock shapes predicted by the present method and reference 2 for a flat plate are shown in figure 13. Good agreement is shown at the angles of attack, 90° and 76° ($M_1 = 20$). The agreement deteriorates somewhat at an angle of attack of 60°. A point to be noted at the angle of attack of 60° with $M_1 = 5$ is the location of the stagnation streamline. The streamline predicted by reference 2 is essentially straight and parallel to the free-stream direction, implying that the stream entered the shock at its apex. This is in contradiction to the assumption made herein that the stagnation streamline should exhibit a subsonic type behavior and curve toward a nearly normal impingement to the body surface as indicated. Unfortunately, no experimental data are available to resolve the difference in these predicted streamlines.

Surface Velocity and Pressure Distributions

A comparison of the velocity distributions for a flat plate at $M_1 = 20$ predicted by the present method and those of reference 2 for a flat plate are shown in figure 14. Good agreement is shown between the predicted (positive) velocities leeward of the stagnation point at the angles of attack, 90° and 76°. There is less agreement between the predicted values when the angle of attack is 60°. The lack of agreement between the predicted values of the (negative) velocities windward of the stagnation point is more pronounced at the angles of attack, 76° and 60°. This lack of good agreement arises partly from the discrepancies between the predicted streamlines, since the windward velocity is very sensitive to the stagnation streamline as the stagnation point approaches the plate (windward) leading edge.

Predicted and experimental pressure distributions over the forward face of various blunt bodies are compared in figure 15. The comparisons are made for axisymmetric bodies since two-dimensional data, particularly for asymmetrical shapes at various angles of attack, are relatively scarce. However, since the method of estimating the pressure distribution is independent of the

dimensionality of the flow, the good agreement shown in figure 15 between the results of the present method, the results presented in reference 5, and the experimental data demonstrates the validity of this method.

CONCLUSIONS

A method has been developed for predicting shock envelopes and pressure distributions for a variety of two-dimensional blunt bodies at various angles of attack. The method is restricted to those cases in which the bow shock is detached from the body and the flow over the forward face of the body is subsonic.

This method utilizes a quickly convergent calculative procedure based on correlation functions which relate the shock standoff distances at the stagnation and sonic points to the body geometry. The correlation functions depend primarily on the normal-shock density ratio modified to a small degree by the specific heat ratio of the gas. Since the effect of the specific heat ratio is small, the method should give adequate solutions for the equilibrium flows of real gases.

Predicted shock envelopes and pressure distributions compared favorably with the results of other theoretical methods and with experimental values in the Mach number range 4.0 to 20.

Ames Research Center
National Aeronautics and Space Administration
Moffett Field, Calif. 94035, Sept. 25, 1972

APPENDIX A

BODY-SHOCK GEOMETRY IN SYMMETRY PLANE

The relationship between the shock and body radii, R_s and R_b, and the shock standoff distance, Δ_{st}, in the plane of symmetry is determined by utilizing mass-flow continuity, oblique shock relationships, and a suitable coordinate system.

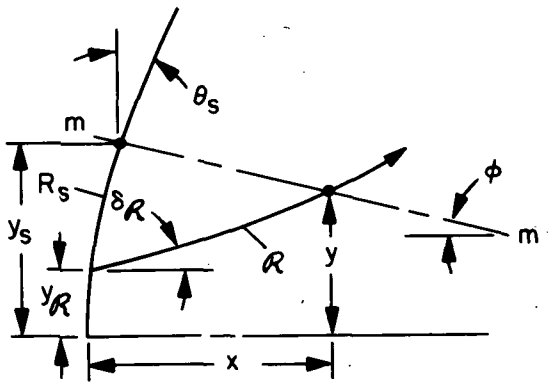

Sketch (e)

Mass flow near the shock—The shock and flow geometry is depicted in sketch (e). The analysis is confined to the domain below a control surface m-m which extends normal to the body surface (not shown). This surface is inclined to the symmetry plane at a small angle, ϕ. The purpose of the following calculations is to find the mass-flow component normal to the plane m-m and its derivative along m-m at the shock.

A streamline entering the curved shock of radius, R_s, at some point, $y_{\mathscr{R}}$, above the shock apex will be deflected an angle, $\delta_{\mathscr{R}}$, and will pursue a curved path of radius, $\mathscr{R}$, behind the shock. The results of reference 8 give the following radius ratio for small θ:

$$\frac{R_s}{\mathscr{R}} = \frac{\rho_2}{\rho_1}\left[\frac{\rho_2}{\rho_1} + \frac{(5 - \gamma)}{(1 + \gamma)}\right]\theta \tag{A1}$$

where $\theta = y/R_s$ and ρ_2/ρ_1 is the normal-shock density ratio.

By oblique shock theory, the small deflection angle $\delta_{\mathscr{R}}$ can be expressed as follows:

$$\delta_{\mathscr{R}} = (y_{\mathscr{R}}/R_s)\left(\frac{\rho_2}{\rho_1} - 1\right) \tag{A2}$$

In the vicinity of the shock, the equation of the streamline entering the shock ($x = 0$) at $y = y_{\mathscr{R}}$ is given by Maclaurin's expansion

$$y = y_{\mathscr{R}}\left\{1 + \left(\frac{\rho_2}{\rho_1} - 1\right)\frac{x}{R_s} + \frac{\rho_2}{2\rho_1}\left[\frac{\rho_2}{\rho_1} + \frac{(5 - \gamma)}{(1 + \gamma)}\right]\left(\frac{x}{R_s}\right)^2\right\} = y_{\mathscr{R}} f(x) \tag{A3}$$

The equation of the control surface, m-m, is

$$y = y_s - \phi x \tag{A4}$$

The inclination of the streamline where it intersects the control surface is $dy/dx + \phi$. Flow continuity along the streamline, $s \approx x$, gives the mass-flow relationship, $\rho V/\rho_1 V_1 = y_{\mathscr{R}}/y$. The component of mass flow normal to m-m is

$$\frac{(\rho V)_n}{\rho_1 V_1} = \frac{y_{\mathscr{R}}}{y}\left(\frac{dy}{dx} + \phi\right) \tag{A5}$$

Equation (A5) is expressed in terms of y_s and x as

$$\frac{(\rho V)_n}{\rho_1 V_1} = \frac{1}{f(x)}\left(\frac{y_s - x}{f(x)}\left\{\frac{\left(\frac{\rho_2}{\rho_1} - 1\right)}{R_s} + \frac{\rho_2}{\rho_1}\left[\frac{\rho_2}{\rho_1} + \frac{(5 - \gamma)}{(1 + \gamma)}\right]\frac{x}{R_s^2}\right\} + \phi\right) \tag{A6}$$

Equation (A6) gives at the shock ($x = 0$)

$$\frac{(\rho V)_n}{\rho_1 V_1} = \delta_s + \phi \tag{A7}$$

The derivative of equation (A6) at $x = 0$ is

$$\frac{d(\rho V)_n}{\rho_1 V_1 dx} = -\frac{2}{R_s}\left(\frac{\rho_2}{\rho_1} - 1\right)(\delta_s + \phi) + \frac{1}{\mathscr{R}} \tag{A8}$$

A two-term expression for the normal mass-flow component in the vicinity of the shock is

$$\frac{(\rho V)_n}{\rho_1 V_1} = (\delta_s + \phi) - \left[\frac{2}{R_s}\left(\frac{\rho_2}{\rho_1} - 1\right)(\delta_s + \phi) - \frac{1}{\mathscr{R}}\right]x \tag{A9}$$

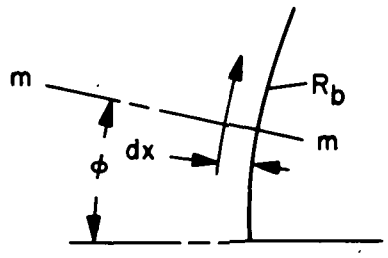

Sketch (f)

Mass flow near the body—A streamline in the vicinity of the stagnation point on the body is shown in sketch (f). At a small distance, dx, from the body, the stream is essentially parallel to the surface.

From equation (3), the mass-flow gradient at the stagnation point of the body is

$$\frac{d(\rho V)_n}{\rho_1 V_1 ds} = \frac{(1 + \Delta_{st}/R_b)}{\Delta_{st}} G \tag{A10}$$

The subscript n has been appended to indicate that the flow at (or near) the body surface is normal to the control surface m-m.

At the point $ds = R_b\phi$ on the body surface, the mass flow is

$$\frac{(\rho V)_n}{\rho_1 V_1} = \frac{(1 + \Delta_{st}/R_b)}{\Delta_{st}} GR_b\phi \tag{A11}$$

Assuming that the circulation $\oint V \cdot ds = 0$ holds for the perimeter of a small concentric strip of width dx and length $R_b\phi$ it can be shown that

$$\frac{d(\rho V)_n}{\rho_1 V_1 dx} = \frac{(1 + \Delta_{st}/R_b)}{\Delta_{st}} G\phi \tag{A12}$$

Normal mass-flow variation along the control surface—A four-term polynomial expression for the variation of normal mass flow from the shock to the body along the control surface m-m is

$$\frac{(\rho V)_n}{\rho_1 V_1} = (\delta_s + \phi) - \left[2\left(\frac{\rho_2}{\rho_1} - 1\right)(\delta_s + \phi)\frac{\Delta_{st}}{R_s} - \frac{\Delta_{st}}{\mathscr{R}}\right]\frac{x}{\Delta_{st}} + C_2\left(\frac{x}{\Delta_{st}}\right)^2 + C_3\left(\frac{x}{\Delta_{st}}\right)^3 \tag{A13}$$

The constants C_2 and C_3 are determined so that $x/\Delta_{st} = 1$ (body surface), equation (A13) reduces to equation (A11) and the derivative of equation (A13) reduces to equation (A12).

Shock and body radius relationship—The normal mass-flow distribution given by equation (A13) was integrated over the interval $0 < x < \Delta_{st}$ to give the total mass flow passing through the control surface m-m and was equated to the flow entering the shock element, $y_s\rho_1 V_1$. Omitting arithmetic details, the following identity resulted:

$$(R_b+\Delta_{st})\phi = \Delta_{st}\left\{\frac{(\delta_s+\phi)}{2}\left[1 - \frac{1}{3}\left(\frac{\rho_2}{\rho_1} - 1\right)\frac{\Delta_{st}}{R_s}\right] + \left(1 + \frac{\Delta_{st}}{R_b}\right)\left(\frac{R_b}{\Delta_{st}} - \frac{1}{6}\right)\frac{G\phi}{2} + \frac{1}{12}\frac{\Delta_{st}}{\mathscr{R}}\right\} \tag{A14}$$

The geometric relationship $y_s/R_s = (\Delta_{st}+R_b)\phi/R_s$ relates δ_s, ϕ, and θ_s. The ratio $\Delta_{st}/\mathscr{R}$ and the angles δ_s and ϕ were thereby eliminated from equation (A14), giving the final result:

$$\left(2 + \frac{\Delta_{st}}{R_b}\right) - \left(1 + \frac{\Delta_{st}}{R_b}\right)\left(1 - \frac{\Delta_{st}}{6R_b}\right)G$$

$$= \left(1 + \frac{2\Delta_{st}}{3R_b}\right)\left(\frac{\rho_2}{\rho_1} - 1\right)\frac{\Delta_{st}}{R_s} - \frac{1}{2}\left(1 + \frac{\Delta_{st}}{R_b}\right)\left[\frac{1}{3}\left(\frac{\rho_2}{\rho_1}\right)^2 - \frac{\gamma+3}{\gamma+1}\left(\frac{\rho_2}{\rho_1}\right) + \frac{2}{3}\right]\left(\frac{\Delta_{st}}{R_s}\right)^2 \tag{6}$$

APPENDIX B

BODY INCLINATION AT THE SONIC POINT

The solution for an infinite shock-density ratio was used to determine the inclination of the sonic point on a conic-section body. The results were then modified to apply to finite shock-density ratios and to nonconical sections by the following procedures.

Conic-Section Body

The inclination angle ϕ^* at the sonic point was determined as a function of the body bluntness parameter B_b using the Busemann solution for an infinite shock-density ratio. Details for the axisymmetric flow solution are presented in appendix A of reference 3. A similar solution for two-dimensional flow gives the following result:

$$(1 - \sin^2\phi^*) - \frac{P^*}{P_{st}} = \frac{1}{(B_b - 1)}\{[(B_b - 1)\sin^2\phi^* + 1]^{3/2} - [(B_b - 1)\sin^2\phi^* + 1]\} \tag{B1}$$

In the present application of equation (B1), the gas was assumed to be perfect. Since the theory requires an infinite shock-density ratio, the value $P^*/P_{st} = 0.607$, appropriate for a gas with $\gamma = 1.0$ and $M_1 = \infty$, was used. The results for $\sin\phi^*$ are normalized by the value for a circular cylinder ($\sin\phi_c^*$ at $B_b = 1$) and are presented in figure 6 as a function of a/b (note $b/a = B_b^{1/2}$). Although the absolute values for $\sin\phi^*$ given by equation (B1) may not be correct for a finite shock-density ratio, it is assumed that the ratio $\sin\phi^*/\sin\phi_c^*$ will not differ greatly from that given by exact theory. Thus, if the value of ϕ_c^* is known for a circular cylinder in a given free-stream flow, the value of ϕ^* for a conic-section body can be determined from figure 6. The values of ϕ_c^* for a circular cylinder by the exact solutions of reference 1 are presented in figure 5.

Nonconic-Section Bodies

If a blunt body does not have a conic section, the parameter B_b is not appropriate. However, the sonic-point location on other types of blunt bodies may be estimated on the basis of the foregoing analysis. To this end, it is assumed that a shock in the form of a conic section is appropriate for all classes of blunt bodies considered here. For example, a blunt body with a rounded corner of radius r is illustrated in sketch (g). When the flow has an infinite shock-density ratio, the shock coincides with the body in the vicinity of the sonic point. If the sonic point is on the rounded corner of the body, the Busemann solution applies if the body corner radius r is equated to the radius of a conic section at the same sonic-point ordinate, y^* (ref. 3):

$$\frac{r}{b} = \frac{1}{1 + (B_b - 1)\sin^3\phi^*} \qquad \text{(B2)}$$

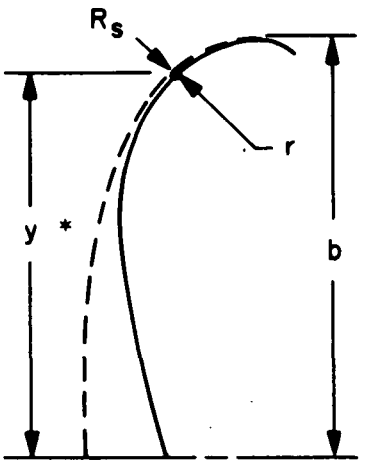

Sketch (g)

Equation (B2) gives the r/b value for an equivalent body that supports the same elliptical shock and the same sonic angle as a body with the bluntness parameter B_b. The value of $\sin\phi^*/\sin\phi_c^*$ for rounded corner bodies as a function of r/b is plotted in figure 6.

In some cases, a qualification of the sonic angle is necessary, for example, when the body is a large-angle wedge or a large-radius surface terminated by a rounded corner. In such cases, the inclined or circularly blunted portion of the body will be tangent to the corner radius r at which point a surface inclination angle $\phi^{t''}$ is defined. The sonic-point angle is then taken as $\phi^{t''}$, if $\phi^{t''}$ is greater than the value of ϕ^* determined from figure 6.

APPENDIX C

ASYMMETRIC STAGNATION STREAM

Streamline Impingement Angle on Body

Consideration is given to a small domain in the vicinity of the stagnation point on the body (sketch (h)). Because of vorticity effects induced by the shock, the stagnation streamline does not impinge normally to the body but will be inclined at some angle Ω with respect to the normal. In this small domain the flow is incompressible and the velocity components will be linearly proportional to the local coordinates, ξ and η. A stream function which yields linear velocity components and satisfies the boundary condition $\psi = 0$ at $\xi = \Omega\eta$ and $\eta = 0$ is

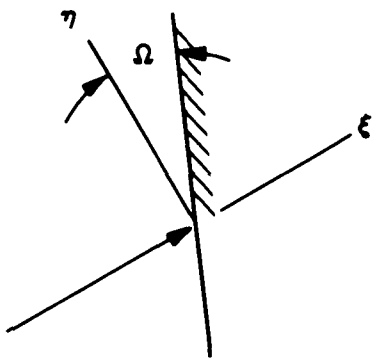

Sketch (h)

$$\psi = C(\xi\eta - \Omega\eta^2) \tag{C1}$$

The velocity gradient $\partial u/\partial \xi$ was assumed constant along the stagnation streamline of length Δ_{st}, and to the order of accuracy required here, was assigned the value

$$\frac{\partial^2 \psi}{\partial \xi \partial \eta} = \frac{\partial u}{\partial \xi} = -\frac{\rho_1}{\rho_2} V_1 \Delta_{st} = C \tag{C2}$$

The vorticity ζ (ref. 9) in terms of the coordinate system used herein is

$$\frac{\partial u}{\partial \eta} - \frac{\partial v}{\partial \xi} = \zeta = V_1 \left(\frac{\rho_2}{\rho_1}\right)\left(1 - \frac{\rho_1}{\rho_2}\right)^2 \frac{\theta_s}{R_s} \tag{C3}$$

where θ_s is the small angle indicated in sketch (e).

Equation (C1) is differentiated partially for ζ, and with the C from (C2), gives

$$\frac{\partial u}{\partial \eta} - \frac{\partial v}{\partial \xi} = \frac{\partial^2 \psi}{\partial \eta^2} + \frac{\partial^2 \psi}{\partial \xi^2} = -2C_\psi \Omega = 2\rho_1 V_1 \Omega / \rho_2 \Delta_{st} \tag{C4}$$

Equations (C3) and (C4) are equated to yield

$$\Omega = \frac{1}{2} \frac{\Delta_{st}}{R_s}\left(\frac{\rho_2}{\rho_1} - 1\right)^2 \frac{y_s}{R_s} \tag{C5}$$

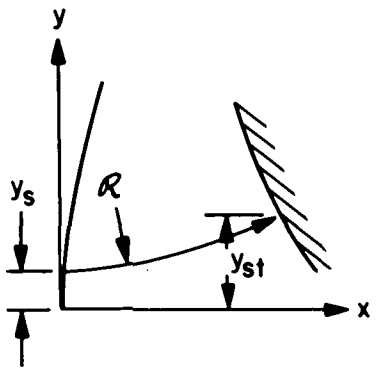

Sketch (i)

Stream Geometry

The stagnation streamline is referenced to a coordinate system whose origin is at the shock "apex" as shown in sketch (i). The streamline ordinate is y_s at the shock and y_{st} at the body.

Examination of incompressible asymmetric flows in general shows that the stagnation streamline increases uniformly in curvature as it approaches the stagnation point. A simple curve having this property was chosen to represent the stagnation streamline between the shock and the body.

$$\mathcal{R} = C_{\mathcal{R}}/\tan \delta \tag{C6}$$

The constant $C_{\mathcal{R}}$ is selected to give the correct streamline radius at the shock as follows:

$$C_{\mathcal{R}} = \mathcal{R}_s \tan \delta_s \tag{C7}$$

The differential streamline length is

$$ds = \frac{C_{\mathcal{R}}\, d\delta}{\tan \delta} \tag{C8}$$

After integrating equation (C8) and evaluating it between the limits δ_s and $\phi_{st} + \Omega$, it is equated to the length of the stagnation streamline, Δ_{st}, to yield

$$\Delta_{st} = \mathcal{R}_s \tan \delta_s \ln\left[\frac{\sin(\phi_{st} + \Omega)}{\sin \delta_s}\right] \tag{C9}$$

Similarly, the ordinate change in the streamline between the shock and the body can be found by integrating $dy = \sin \delta\, ds = C_{\mathcal{R}} \cos \delta\, d\delta$:

$$y_{st} - y_s = R_s \tan \delta_s [\sin(\phi_{st} + \Omega) - \sin \delta_s] \tag{C10}$$

The term R_s can be eliminated between equations (C9) and (C10) and, using the relationship $\delta_s = [(\rho_2/\rho_1)-1](y_s/R_s)$, the following streamline ordinate relationship results:

$$\frac{y_{st} - y_s}{\Delta_{st}} = \frac{\sin(\phi_{st} + \Omega) - \sin \delta_s}{\ln \dfrac{\sin(\phi_{st} + \Omega)}{\sin \delta_s}} \tag{C11}$$

Equations (C5) and (C11) were used to calculate values of y_s and y_{st} as functions of Δ_{st}/R_s, ϕ_{st}, and ρ_2/ρ_1. The results are presented in figure 9.

APPENDIX D

AUXILIARY INSTRUCTIONS FOR TABLE 2

The computing form (table 2) for determining the velocity correction term applies directly to a body consisting of three finite tangent radii, R_b, r^t, and r (items (1) to (3)) between the stagnation and sonic point locations (sketch (j)). The angles ϕ_{st}, $\phi^{t'}$, $\phi^{t''}$, and ϕ^* (items (4) to (7)) measure in radians the surface inclinations at the stagnation point, the tangent points, and the sonic point with respect to a plane normal to the free-stream direction. In cases where any of the surface element radii are of zero curvature, the distances $s^{t'}$, $s^{t''}$, and s^* to the tangent points (items (8) to (10)) as specified in the computing form are indeterminate. In this event, the following auxiliary equations for computing the values of s are required. For clarification, the geometry for each of the following cases is shown in sketch (k).

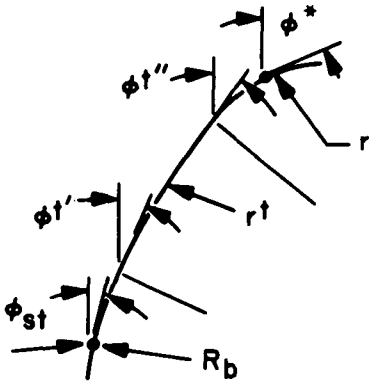

Sketch (j)

Case I, $R_b = \infty$, r^t and r Finite

Since the angle $\phi_{st} = \phi^{t'}$, the value of $s^{t'}$ (item (8)) is

$$s^{t'} = y^* - \frac{r^t(\sin \phi^{t''} - \sin \phi_{st}) - r(\sin \phi^* - \sin \phi^{t''})}{\cos \phi_{st}} \tag{D1}$$

Case II, $r^t = \infty$, R_b and r Finite

Since the angle $\phi^{t'} = \phi^{t''}$, the value of $s^{t''}$ (item (9)) is

$$s^{t''} = s^{t'} + \frac{y^* - R_b(\sin \phi^{t'} - \sin \phi_{st}) - r(\sin \phi^* - \sin \phi^{t'})}{\cos \phi^{t'}} \tag{D2}$$

Case III, $r = \infty$, R_b and r^t Finite

Since the angle $\phi^{t''} = \phi^*$, the value of s^* (item (10)) is

$$s^* = s^{t''} + \frac{y^* - R_b(\sin \phi^{t'} - \sin \phi_{st}) - r^t(\sin \phi^* - \sin \phi^{t'})}{\cos \phi^*} \tag{D3}$$

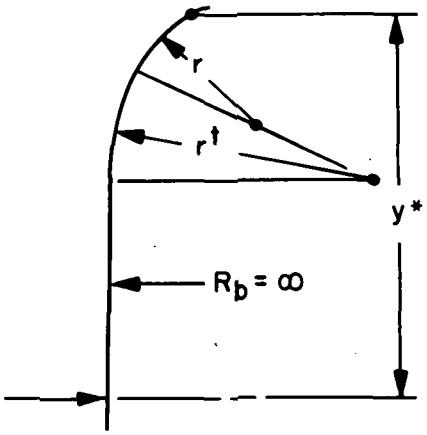

Case I

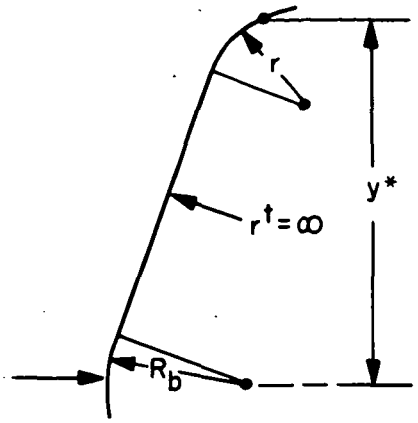

Case II

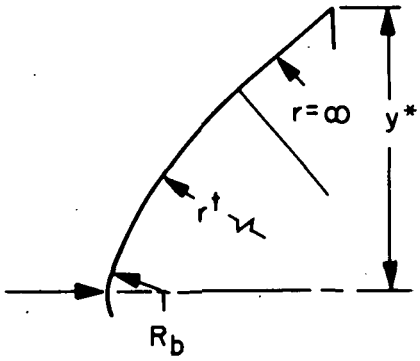

Case III

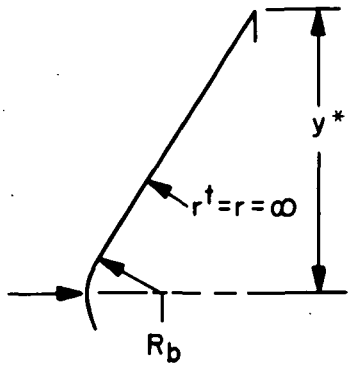

Case IV

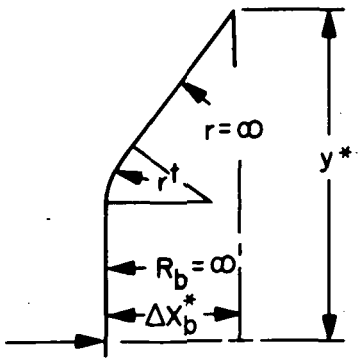

Case V

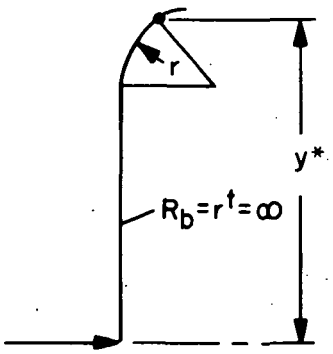

Case VI

Sketch (k)

Case IV, R_b Finite, $r^t = r = \infty$

Since the angles $\phi^{t'} = \phi^{t''} = \phi^*$ and the value of $s^{t''} = s^*$ (item (9) equals item (10)),

$$s^{t''} = s^* = s^{t'} + \frac{y^* - R_b(\sin \phi^* - \sin \phi_{st})}{\cos \phi^*} \tag{D4}$$

Case V, r^t Finite, $R_b = r = \infty$

Since the angle $\phi_{st} = \phi^{t'}$ and the angle $\phi^{t''} = \phi^*$, the value of $s^{t'}$ (item (8)) is

$$s^{t'} = \frac{y^* \sin \phi^* - \Delta x_b^* \cos \phi^{t'} - r^t[1 - \cos(\phi^* - \phi_{st})]}{\sin(\phi^* - \phi_{st})} \tag{D5a}$$

where Δx_b^* is the horizontal distance between the stagnation and the sonic point locations.

The value of s^* (item (10)) is

$$s^* = s^{t''} + \frac{y^* - s^{t'} \cos \phi_{st} - r^t(\sin \phi^* - \sin \phi_{st})}{\cos \phi^*} \tag{D5b}$$

Case VI, $R_b = r^t = \infty$, r = Finite

Since the angles $\phi_{st} = \phi^{t'} = \phi^{t''}$, the value of $s^{t'} = s^{t''}$ (item (8) equals item (9)) is

$$s^{t'} = s^{t''} = \frac{y^* - r(\sin \phi^* - \sin \phi_{st})}{\cos \phi_{st}} \tag{D6}$$

Scale Factor

The "smoothed" Newtonian velocity distribution, equation (43), is not generally equal to that of the velocity distribution given by equation (42). It is assumed, however, that the incremental velocity distribution, accounting for the effect of surface curvature discontinuities by Newtonian theory (item (25)), is qualitatively valid and by an appropriate scaling factor can be applied as an additive correction term to the "smooth" velocity distribution given by equation (42). A logical scaling factor, f, is the ratio of the velocity gradients, $f = \dot{\bar{V}}/\dot{\bar{v}}$, where $\dot{\bar{V}}$ and $\dot{\bar{v}}$ are the respective gradients of equations (42) and (43). Preferably, the gradients should be evaluated at the stagnation point, whence

$$f = \dot{\bar{V}}(0)/\dot{\bar{v}}(0) \tag{D7}$$

The term $\dot{\bar{V}}(0)$ is given by equation (35) and $\dot{\bar{v}}(0) = s^*/R_b$ is item (11) in the computing form.

In the case when $R_b = \infty$, the Newtonian value, $\dot{\bar{v}}(0) = 0$, is not realistic. An alternative choice is then the velocity gradient ratio at the sonic point:

$$f = \frac{\dot{\bar{V}}(1)}{\dot{\bar{v}}(1)} = \frac{P_{st}}{\gamma P^*} \tag{D8}$$

REFERENCES

1. Fuller, Franklyn B.: Numerical Solutions for Supersonic Flow of an Ideal Gas Around Blunt Two-Dimensional Bodies. NASA TN D-791, 1961.

2. Bazhin, A. P.: On Calculation of Supersonic Flow of Gas Over a Thin Flat Plate With a Detached Shock Wave. Engineering J., No. 2, Aug. 1964, pp. 31-39.

3. Kaattari, George E.: A Method for Predicting Shock Shapes and Pressure Distributions for a Wide Variety of Blunt Bodies at Zero Angle of Attack. NASA TN D-4539, 1968.

4. Traugott, Stephen C.: An Approximate Solution of the Direct Supersonic Blunt-Body Problem for Arbitrary Axisymmetric Shapes. J. Aero. Sci., vol. 27, no. 5, May 1960, pp. 361-370.

5. South, Jerry C., Jr.: Calculation of Axisymmetric Supersonic Flow Past Blunt Bodies With Sonic Corners, Including a Program Description and Listing. NASA TN D-4563, 1968.

6. Stallings, Robert L., Jr.: Experimentally Determined Local Flow Properties and Drag Coefficients for a Family of Blunt Bodies at Mach Numbers From 2.49 to 4.63. NASA TR R-274, 1967.

7. Inouye, Mamoru; Marvin, Joseph G.; and Sinclair, A. Richard: Comparison of Experimental and Theoretical Shock Shapes and Pressure Distributions on Flat-Faced Cylinders at Mach 10.5. NASA TN D-4397, 1968.

8. Rakich, John V.; and Menees, Gene P.: A Theoretical and Experimental Study of Hypersonic Flow Over Flared Bodies at Incidence. NASA TN D-3218, 1966.

9. Hayes, Wallace D.; and Probstein, Ronald F.: Hypersonic Flow Theory. Academic Press, New York, 1959, p. 151.

TABLE 1.- SHOCK SOLUTION COMPUTING FORM

1	c (chord) = 1.00	7	$(①-②-④)\cos⑥$ = 0.359	13	$\left(\frac{\Delta^*}{y^*}\right)_p$, fig. 3 = 0.608
2	r_u = 0.10	8	$Y_m = ⑦\tan⑥+②$ = 0.870	14	θ_p^*, fig. 4 = 19.45
3	ε_u = 10°	9	$M_1 = \infty$	15	ϕ_c^*, fig. 5 = 44.5
4	r_ℓ = 0.05	10	γ = 1.4	16	$\phi_u^t = ⑥+③-90° = -15°$
5	ε_ℓ = 16.5°	11	$\frac{\rho_2}{\rho_1} = \left[1+⑩\right]/\left[⑩-1-\frac{2}{⑨^2}\right] = 6$	17	$\phi_\ell^t = 90° +⑤-⑥ = 41.5°$
6	α = 65°	12	G, fig. 1 = 0.966	18	$\frac{1}{2}-\left(\frac{1}{2}-\frac{②}{①}\right)\left(\frac{90°-⑥}{③+⑮}\right) = 0.317$

	Iteration number	0	1	2
19	Initial b = ⑱①	0.317	⑦0.291	⑦0.292
20	r_u/b = ②/⑲	.316	.344	
21	⑳ &fig.6, $\frac{\sin\phi^*}{\sin\phi_c^*}$	.77	.79	
22	$\phi^* = \sin^{-1}($ ㉑ sin ⑮)	32.7	33.6	
23	ϕ_u^* = larger of ㉒ & ⑯	32.7	33.6	
24	Y_u^* = ⑧-②(1-sin ㉓)	.824	.825	
25	X_u^* = ⑦+② cos ㉓	.443	.442	
26	sin ㉓ /sin ⑮	.77	.79	
27	㉖ &fig.7, $\frac{\Delta^*}{y^*}-\left(\frac{\Delta^*}{y^*}\right)_p$	.109	.115	
28	㉖ & fig.8, $\theta^*-\theta_p^*$	-2.60°	-2.55°	
29	$\left(\frac{\Delta^*}{y^*}\right)_u$ = ⑬ + ㉗	.717	.723	
30	θ_u^* = ⑭ + ㉘	16.85°	16.90°	
31	r^2/b = ④/(④+⑧-⑲)	.083	.080	
32	㉛ &fig.6, $\frac{\sin\phi^*}{\sin\phi_c^*}$	.520	.510	
33	$\phi^* = \sin^{-1}($ ㉜ sin ⑮)	21.4	20.9	
34	ϕ_ℓ^* = larger of ㉝ & ⑰	41.5	41.5	
35	Y_ℓ^* = -④sin ㉞	-.033	-.033	
36	X_ℓ^* = ④ cos ㉞	.037	.037	
37	sin ㉞ /sin ⑮	.945	.945	
38	㊲ &fig.7, $\frac{\Delta^*}{y^*}-\left(\frac{\Delta^*}{y^*}\right)_p$	.165	.165	
39	㊲ &fig.8, $\theta^*-\theta_p^*$	-1.30°	-1.30°	
40	$\left(\frac{\Delta^*}{y^*}\right)_\ell$ = ⑬ + ㊳	.773	.773	
41	θ_ℓ^* = ⑭ + ㊴	18.15°	18.15°	
42	y_u^* = ㉔ + ⑲ -⑧	.271	.246	
43	Δ_u^* = ㉙㊷	.194	.178	
44	app. $\left(\frac{x^*}{y^*}\right)_u$ = tan(㉚ /2)	.148	⑥0.121	⑥0.125
45	x_u^* = ㊹㊷	.040	.030	
46	X_s = ㊺ + ㊸ + ㉕	.677	.650	
47	Y_s = ⑧- ⑲	.553	.579	

		0	1	2
48	Δ_0 } Scaled from fig.10 at coordinates ㊻ - ㊼	0.277	0.240	
49	ϕ_0 }	21°	20°	
50	R_b }	1.92	1.92	
51	Δ_{st} = ㊽ (1+cos ㊾)/2	.268	.233	
52	Δ_{st}/R_b = ㊶ / ㊿	.140	.121	
53	㊷ &fig.2. Δ_{st}/R_s	.200	.201	
54	26.7[㊽ sin ㊾] / ㊿	1.4°	1.1°	
55	ϕ_{st} = ㊾ - ㊹	19.6°	18.9°	
56	㊸ & ord. fig.9(a)	.180	.178	
57	y_s = ㊻㊶ sin ㊺	.016	.013	
58	R_s = ㊶ / ㊸	1.340	1.159	
59	1+[㊽ tan ㉚] / ㊷	2.493	2.431	
60	$\left(\frac{x^*}{y^*}\right)_u$ =[tan ㉚] / ㊾ to ㊹ ⑥0	.121	.125	
61	y_ℓ^* = ㊼ - ㉟	.586	.612	
62	1+[㊽ tan ㊶]/ ㊶	1.750	1.621	
63	$\left(\frac{x^*}{y^*}\right)_\ell$ = tan ㊶ / ㊷	.187	.202	
64	Δ_u^* = (㊷ - ㊼) ㉙	.183	.169	
65	Δ_ℓ^* = (㊶ + ㊼) ㊵	.465	.483	
66	㉕ + ㊷㊿ + ㊹	.659	.642	
67	㊱ + ㊶㊸ + ㊺	.612	.644	
68	$X_\ell^t - X_u^t$ = ㊼ - ㊻	-.047	.002	
69	㉙ + ㊵ + ㊿ + ㊸	1.798	1.823	
70	∇ = ㊽ / ㊾	-.026	.001	
71	b = ⑲ + ㊿ to ⑲ ⑦1	.291	.292	
72	㊸ and ord. fig.9(b)			0.680
73	Y_{st} = ㊼ + ㊷㊶ sin ㊺			.630
74	B_{su} = (㊽ / ㊷)^2=cot^2 ㉚			11.36
75	$B_{s\ell}$ = (㊽ / ㊶)^2-cot^2 ㊶			-5.72

TABLE 2.- COMPUTING FORM FOR VELOCITY INCREMENT, $\Delta\bar{V}$

1	$R_b=1.0$	11	$s^*/R_b = (10)/(1) = 4.564$
2	$r^t=\infty$	12	$s^*/r^t = (10)/(2) = 0$
3	$r=\infty$	13	$s^*/r = (10)/(3) = 0$
4	$\phi_{st}=0^a$	14	$C' = (5)-(4)-(8)/(2) = 0.524$
5	$\phi^{t'}=0.524$	15	$n' = \dfrac{(11)-(12)}{(14)} = 8.70$
6	$\phi^{t''}=0.524$	16	$C'+C'' = (7)-(4)-(12) = 0.524$
7	$\phi^*=0.524$	17	$C'' = (16)-(14) = 0$
8	$s^{t'} = ((5)-(4))(1) = 0.524$	18	$n'' = \dfrac{(13)-(12)}{(17)} = 0$
9	$s^{t''} = (8)+((6)-(5))(2) = 4.564$	19	$\bar{v}_B(1) = (14)+(12)+(4) = 0.524$
10	$s^* = (9)+((7)-(6))(3) = 4.564$		

20	21	22	23	24	25	$\Delta\bar{V}$
$\bar{s}$	(20)(18)	$\Delta\bar{v}''=(17)(21)$	$\bar{v}=(22)+(31)$	Line function	(24) - (23)	f (25) [b]
0	1.0	0	0	(4)=0	0	0
0.04			0.157	0.183	0.026	0.016
.08			.281	.366	.085	.054
(8)/(10) =0.1146			.343	(5)=0.524	.179	.114
.15			.397	.524	.127	.081
.25			.476	.524	.048	.031
(9)/(10) =1.0			.524	(6)=0.524	0	0
.60			.524	.524	-	-
.80			.524	.524	-	-
1.0			.524	(7)=0.524	0	0

20	26	27	28	29	30	31
$\bar{s}$	1-(20)	(26)(15)	$\Delta\bar{v}'=(14)(27)$	$v_B(1)-v_B = (12)(26)$	(28) + (29)	$v_B-\Delta\bar{v}' = (19)-(30)$
0	1.000	1.00	0.524	0	0.524	0
.04	.96	.701	.367		.367	0.157
.08	.92	.484	.253		.253	.281
.1146	.8854	.346	.181		.181	.343
.15	.85	.243	.127		.127	.397
.25	.75	.092	.048		.048	.476
1.00	0	0	0		0	.524
.60	.40	-	-		-	.524
.80	.20	-	-		-	.524
1.00	0	0	0		-	.524

[a]Note: ϕ, in radians.

[b]Scaling factor f = 0.64, equation (D7) or (D8).

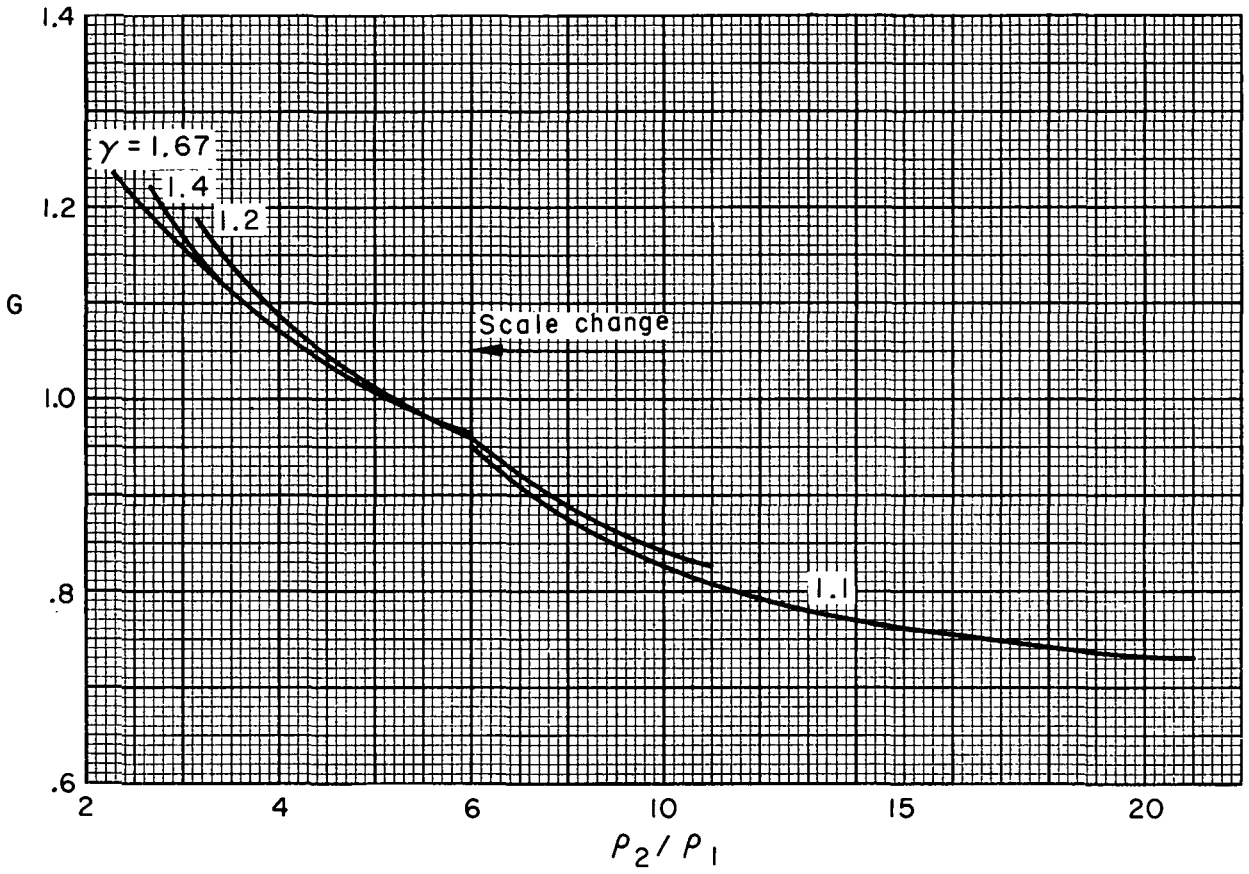

Figure 1.- The G function.

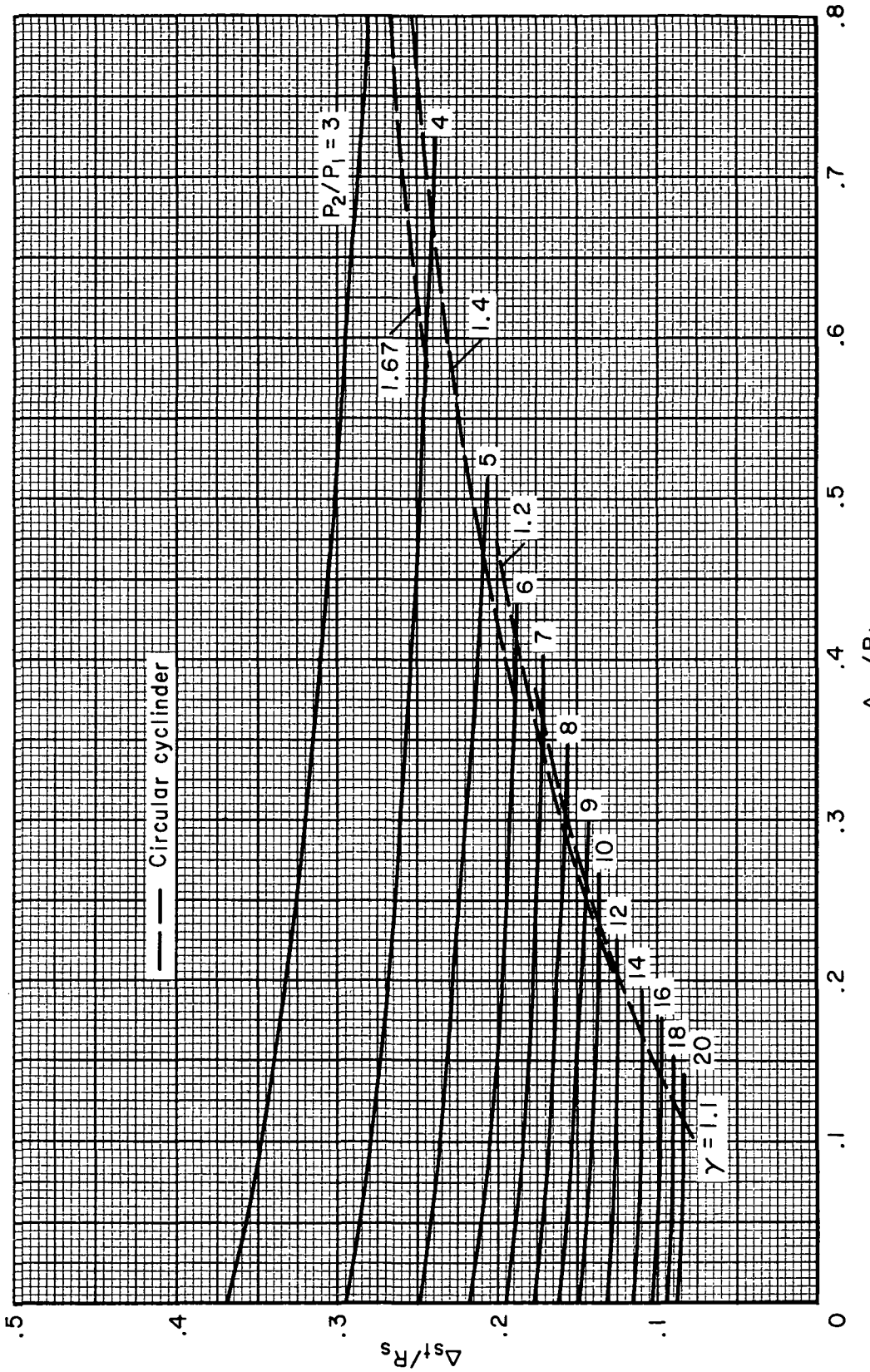

Figure 2.- Values of Δ_{st}/R_s as a function of Δ_{st}/R_b for various values of ρ_2/ρ_1.

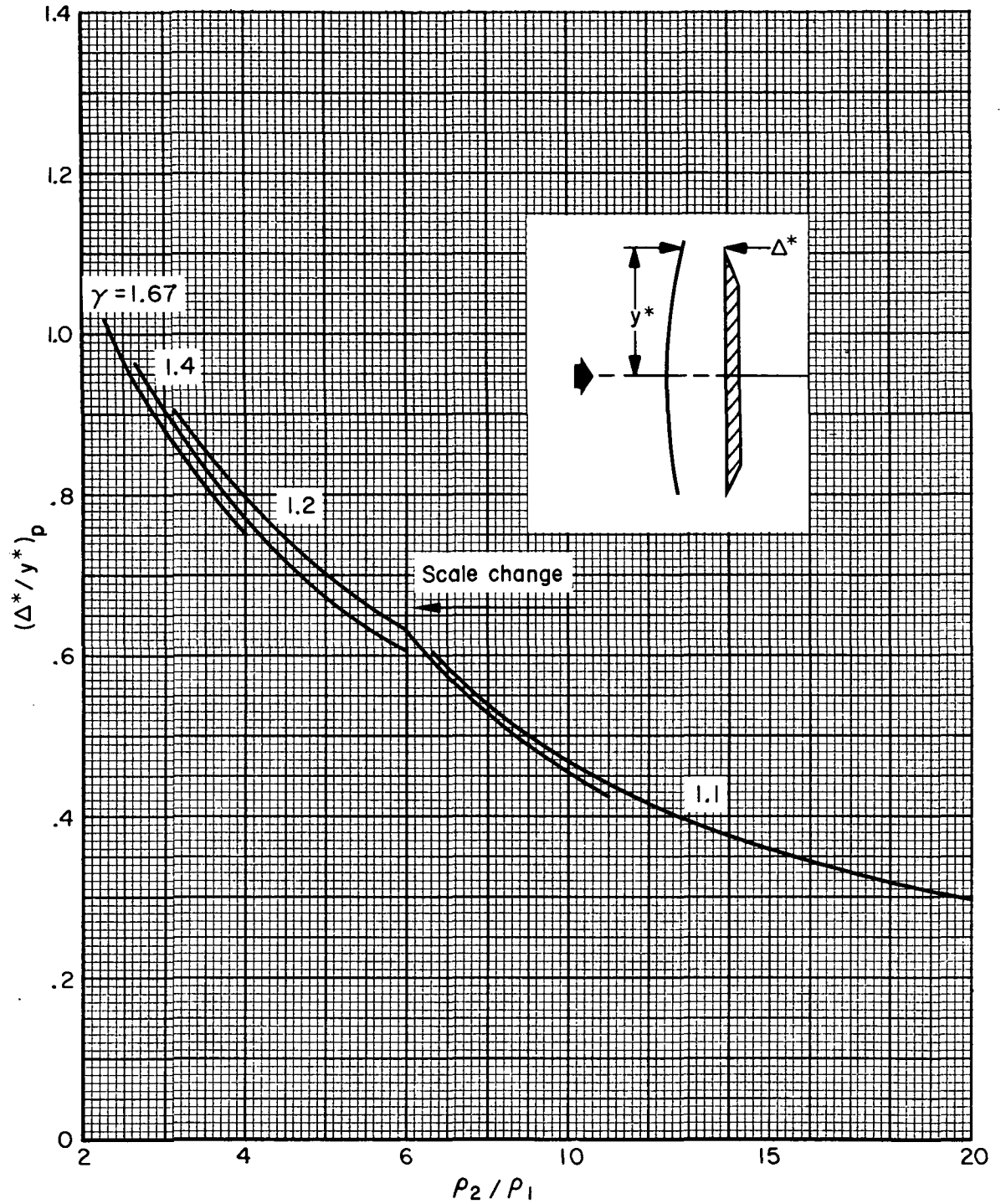

Figure 3.- Sonic-point standoff distance $(\Delta^*/y^*)_p$ for a flat plate normal to the stream.

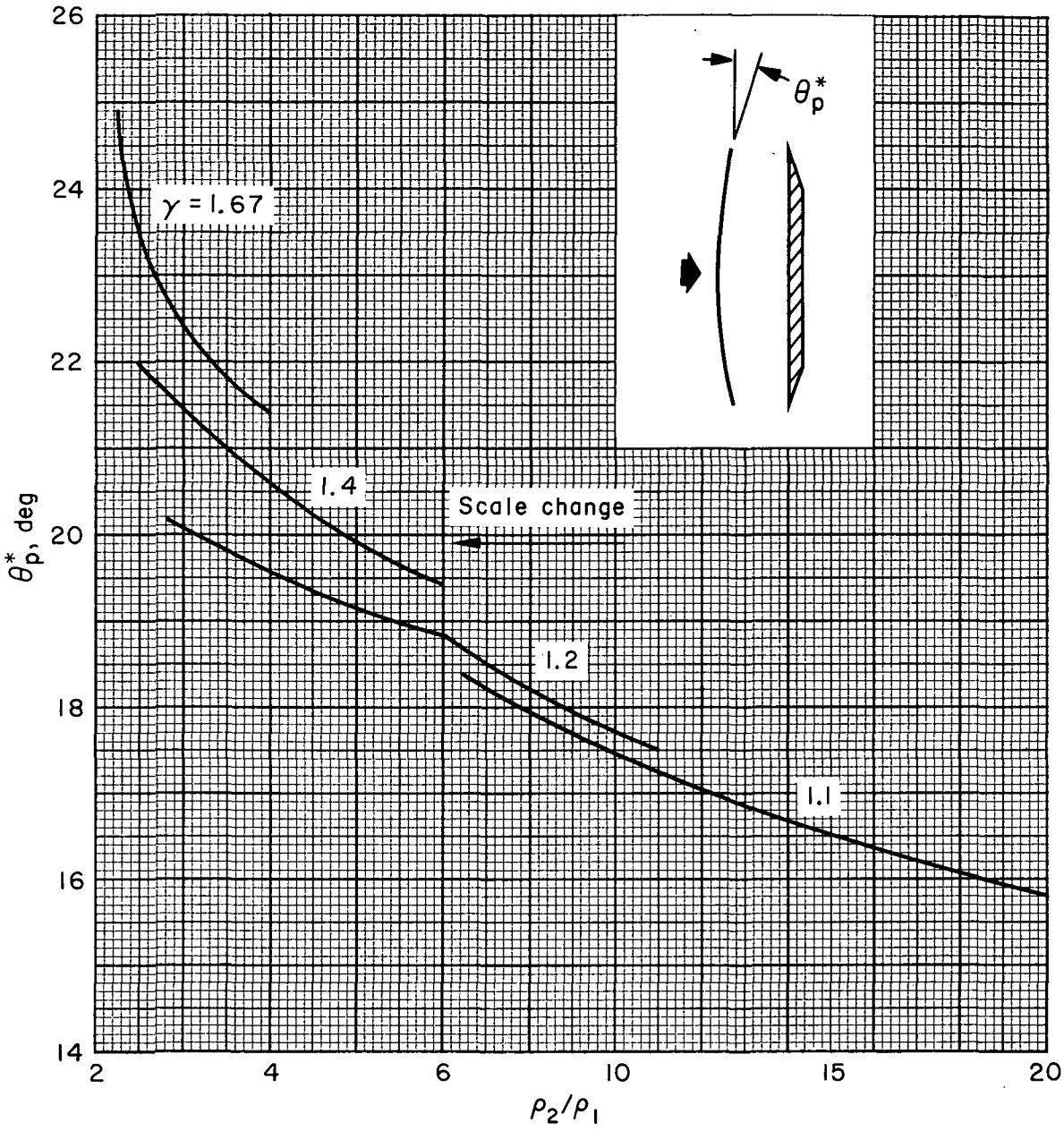

Figure 4.- Shock inclination angle θ_p^* for a flat plate normal to stream.

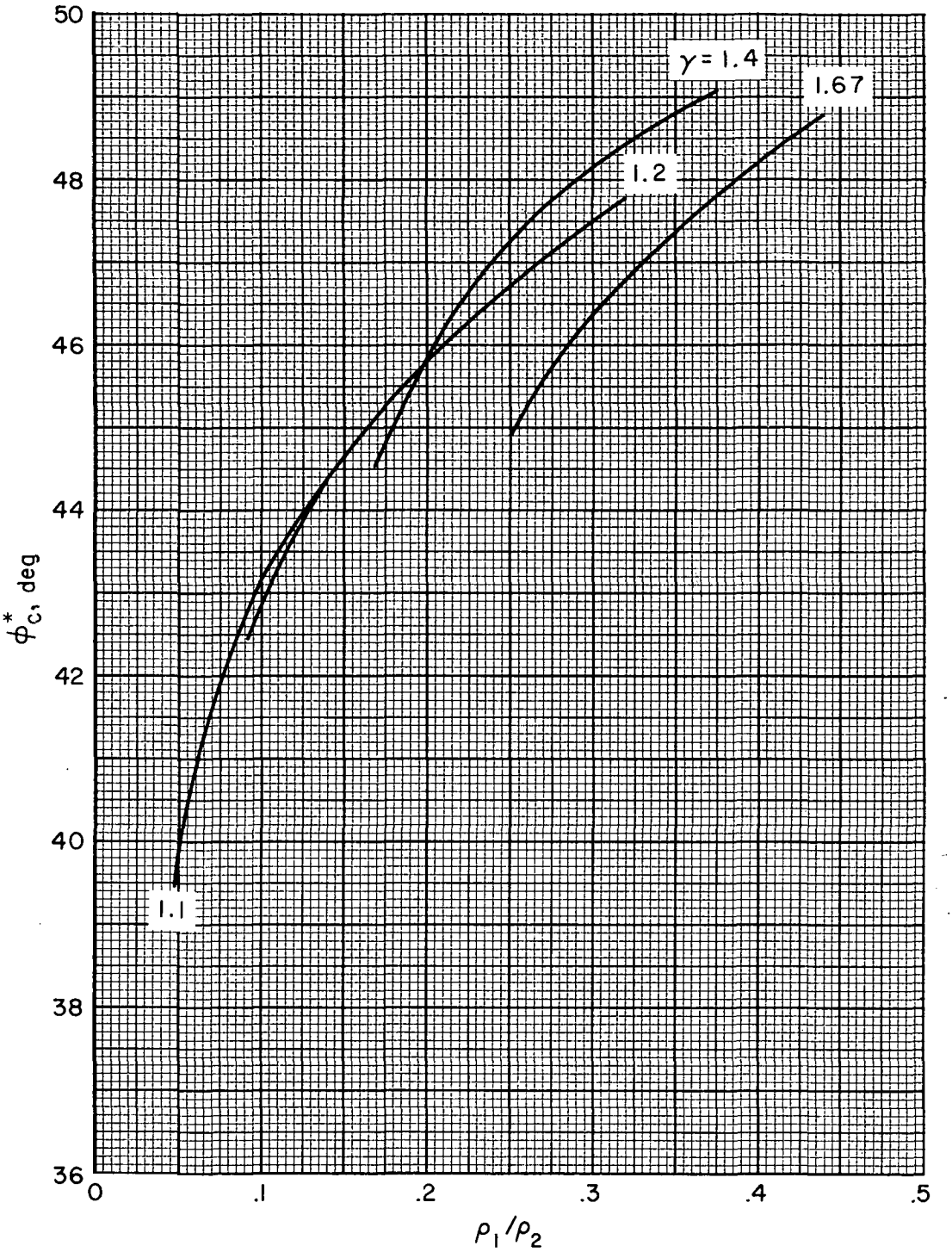

Figure 5.- Sonic-point angle ϕ_c^* on circular cylinder.

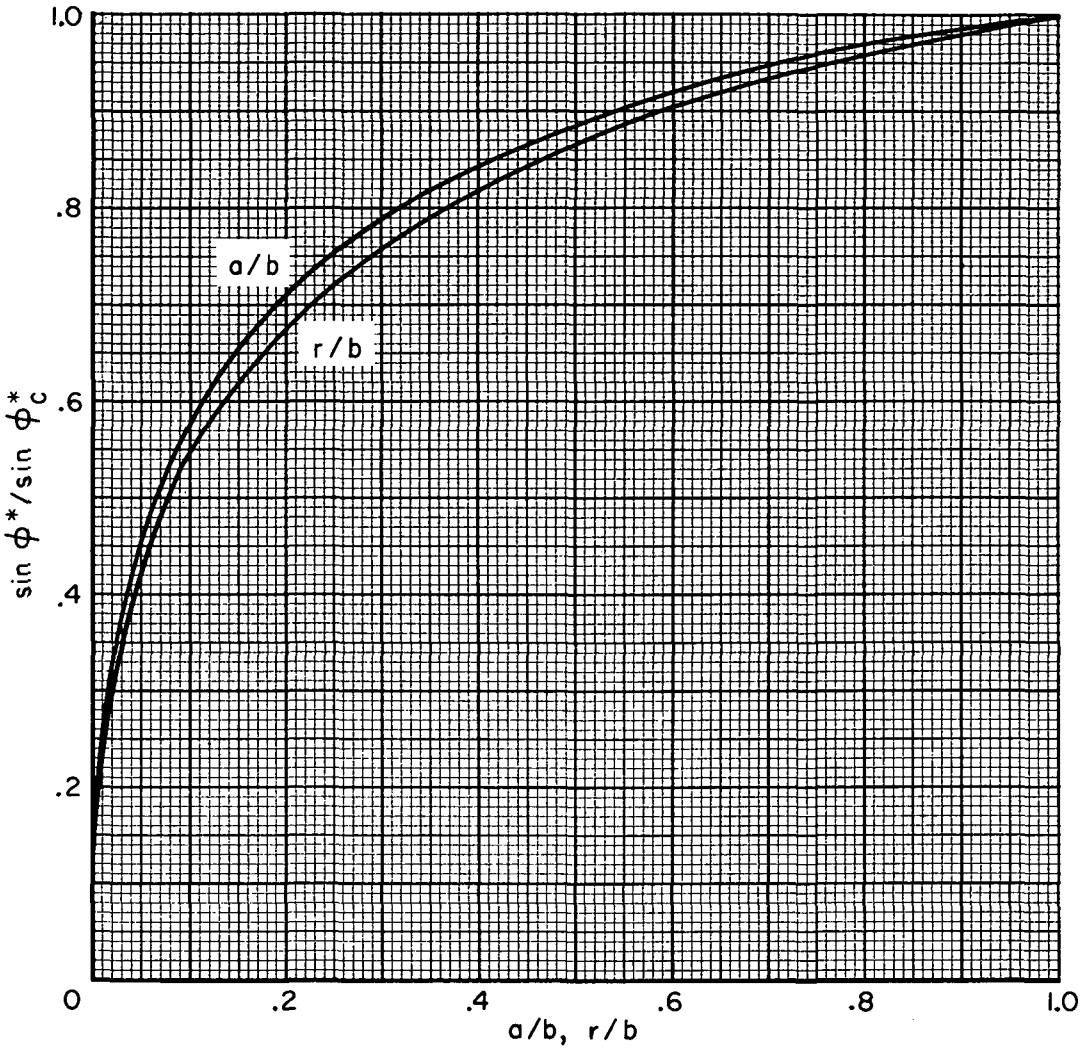

Figure 6.- Sonic-point angle ϕ^* on elliptic and round-corner slab sections.

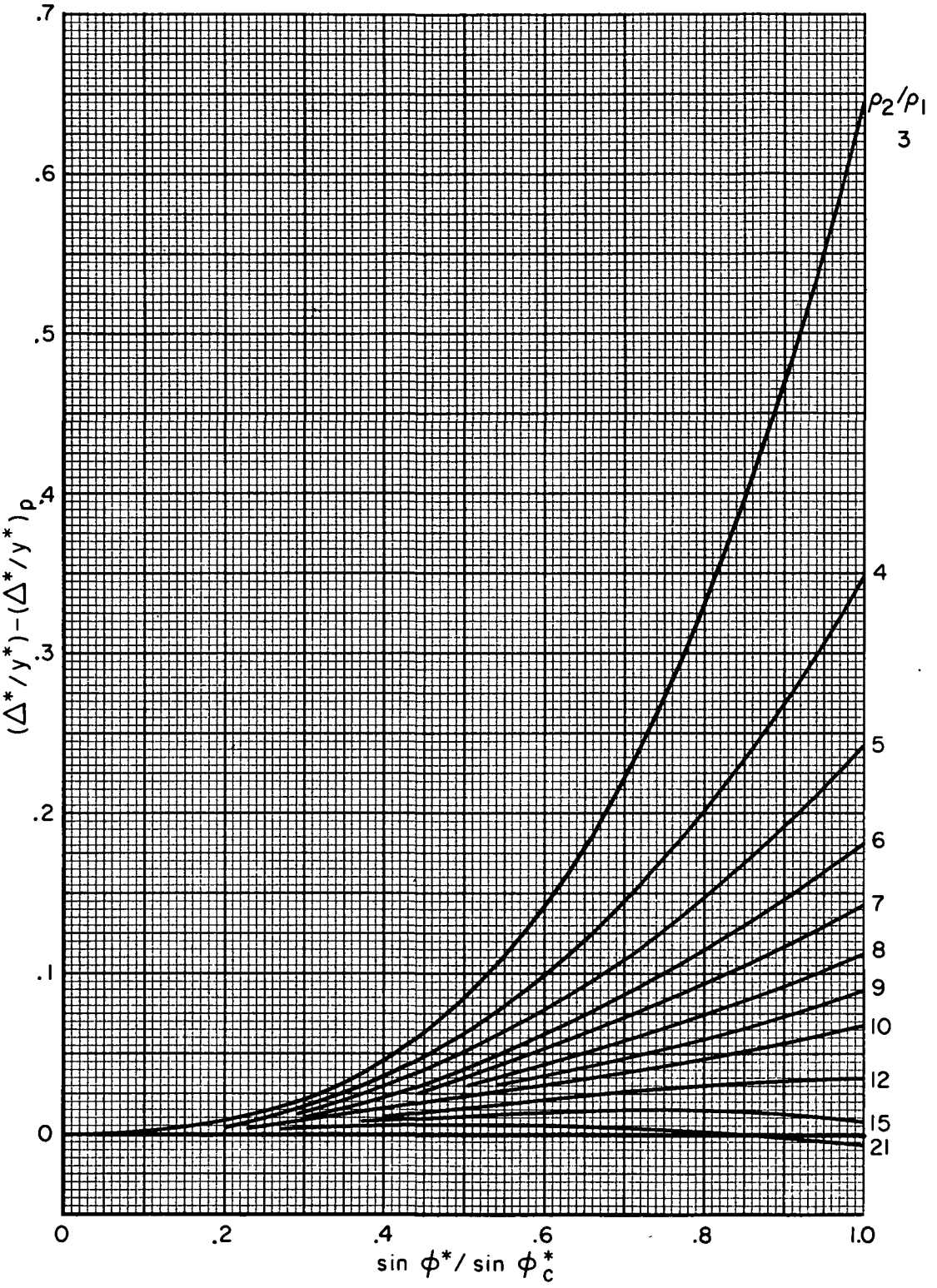

Figure 7.- Values of $(\Delta^*/y^*) - (\Delta^*/y^*)_p$ as a function of $\sin \phi^*/\sin \phi_c^*$.

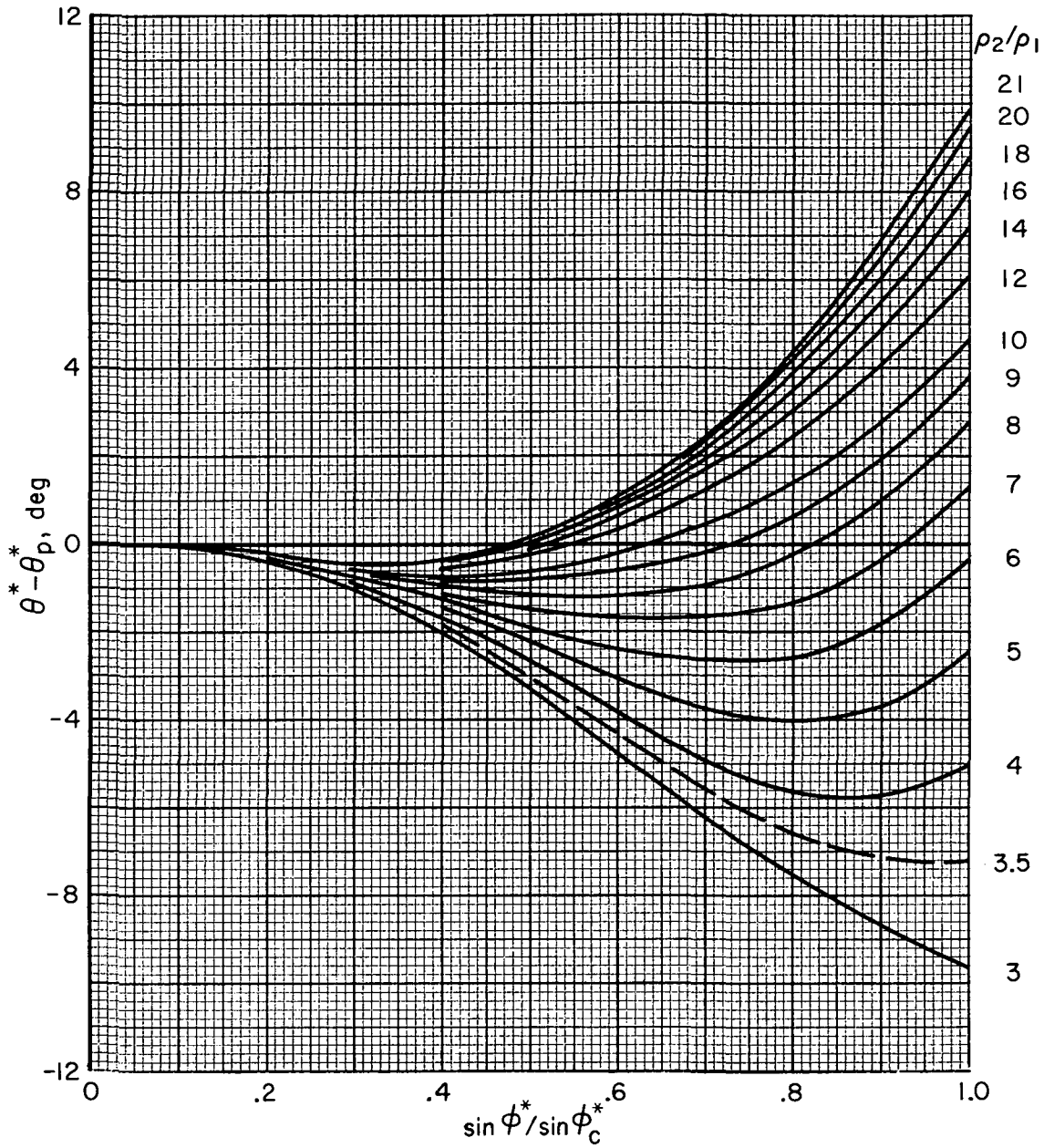

Figure 8.- Values of $\theta^* - \theta_p^*$ as a function of $\sin \phi^* / \sin \phi_c^*$.

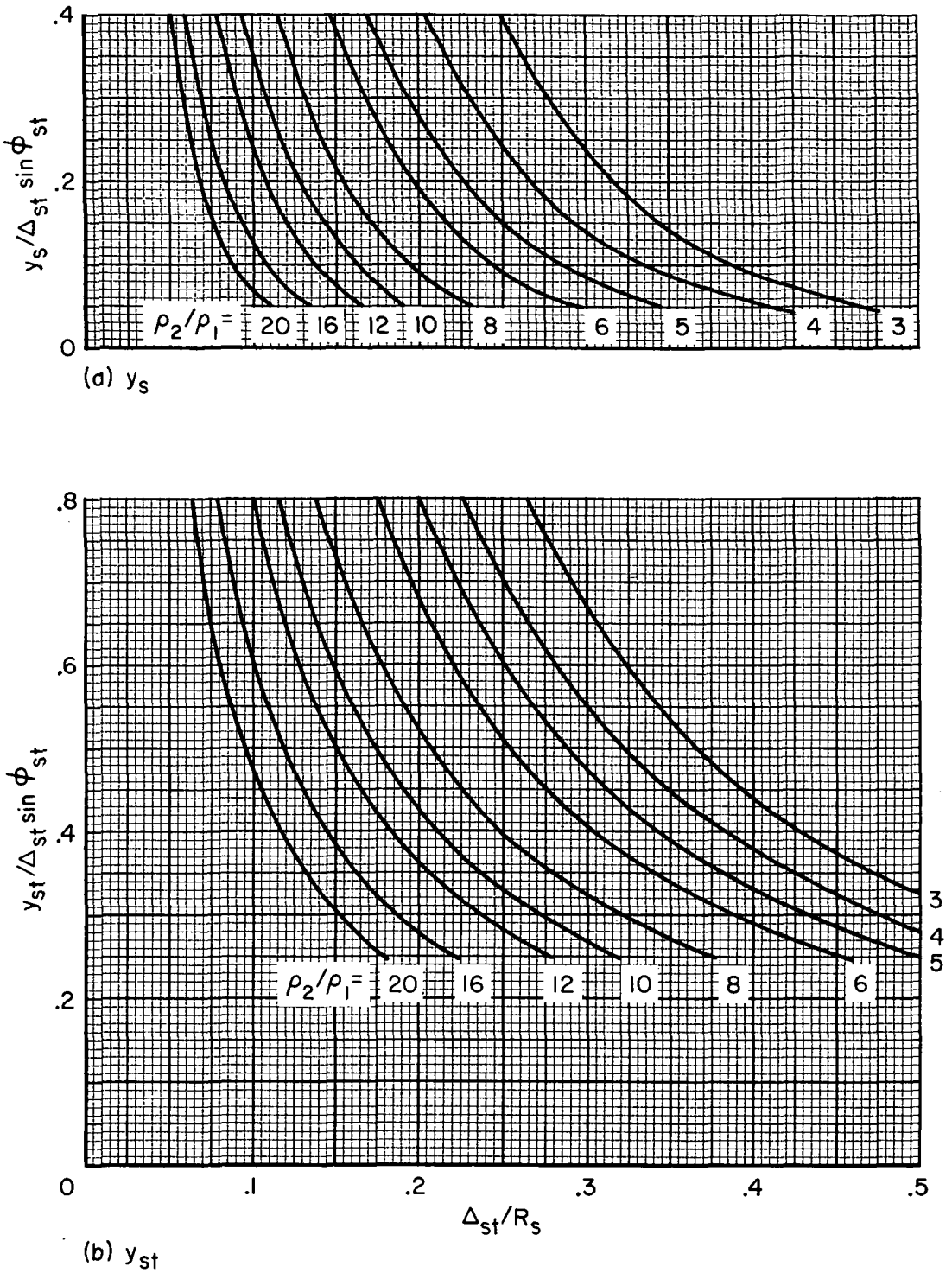

Figure 9.- Streamline displacement, y_s and y_{st}.

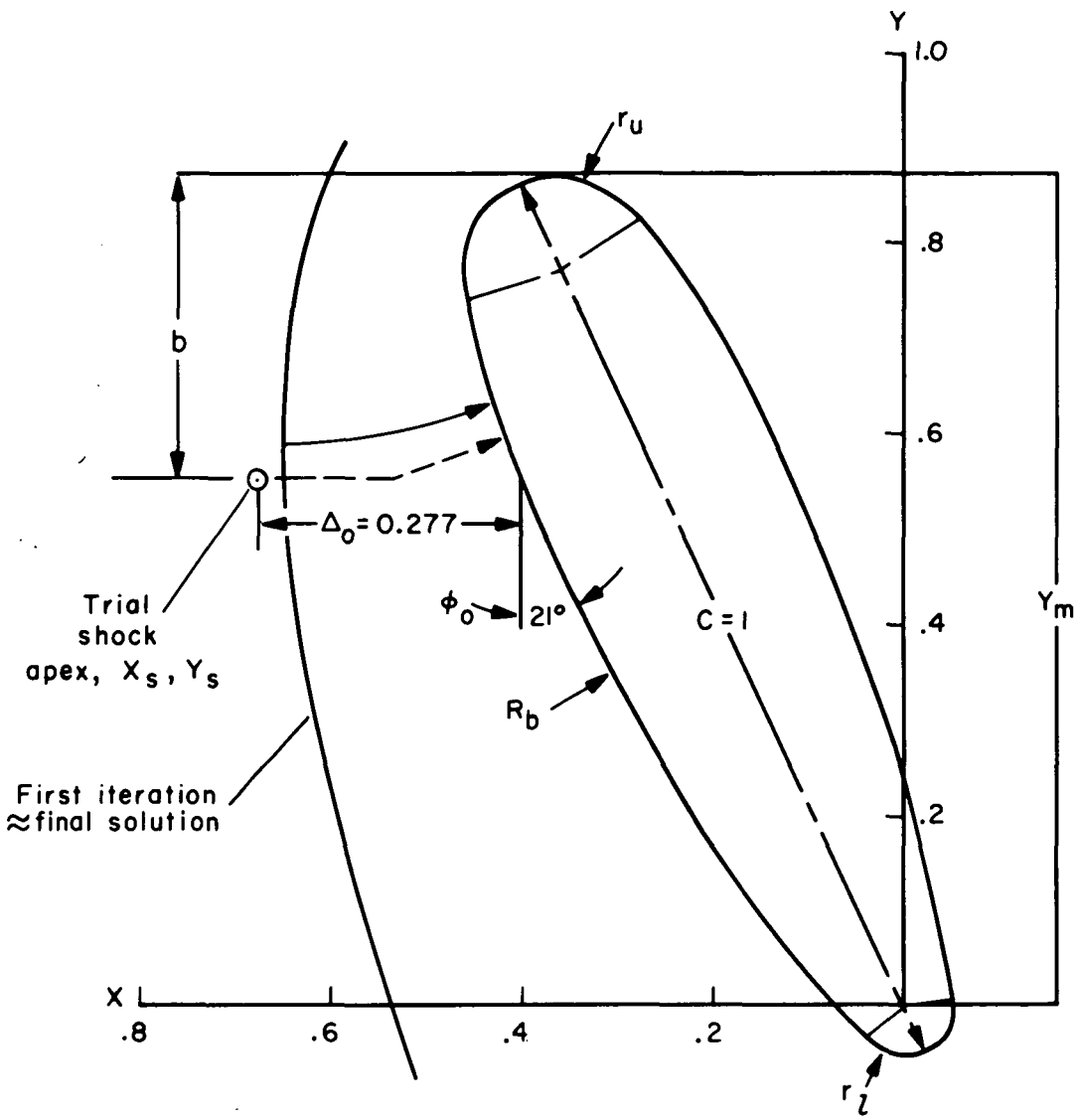

Figure 10.- Coordinate system for shock solution with example solution.

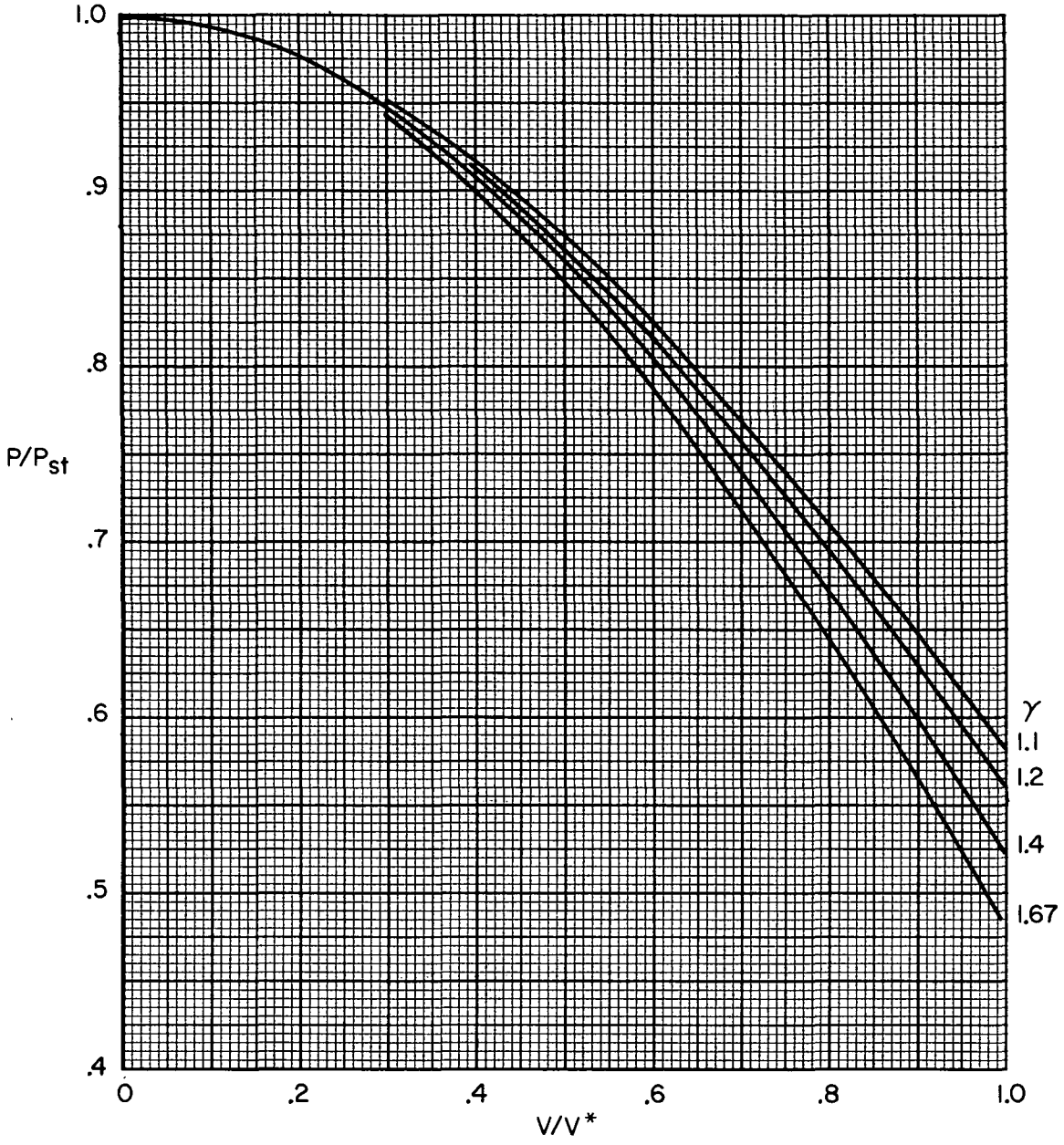

Figure 11.- The ratio p/p_{st} as a function of $V/\forall^*$.

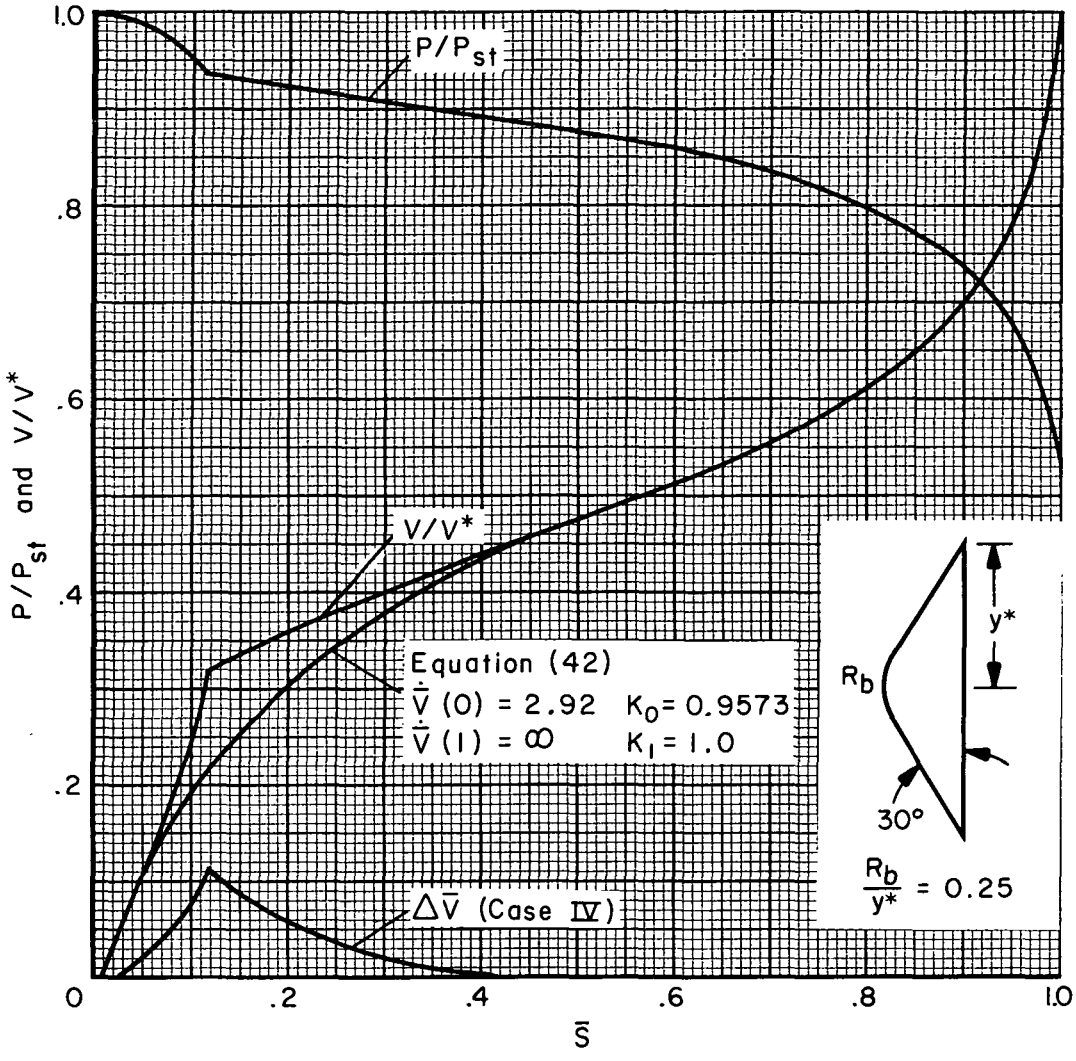

Figure 12.- Sample numerical results for a blunted cone, $M_1 = 4.86$.

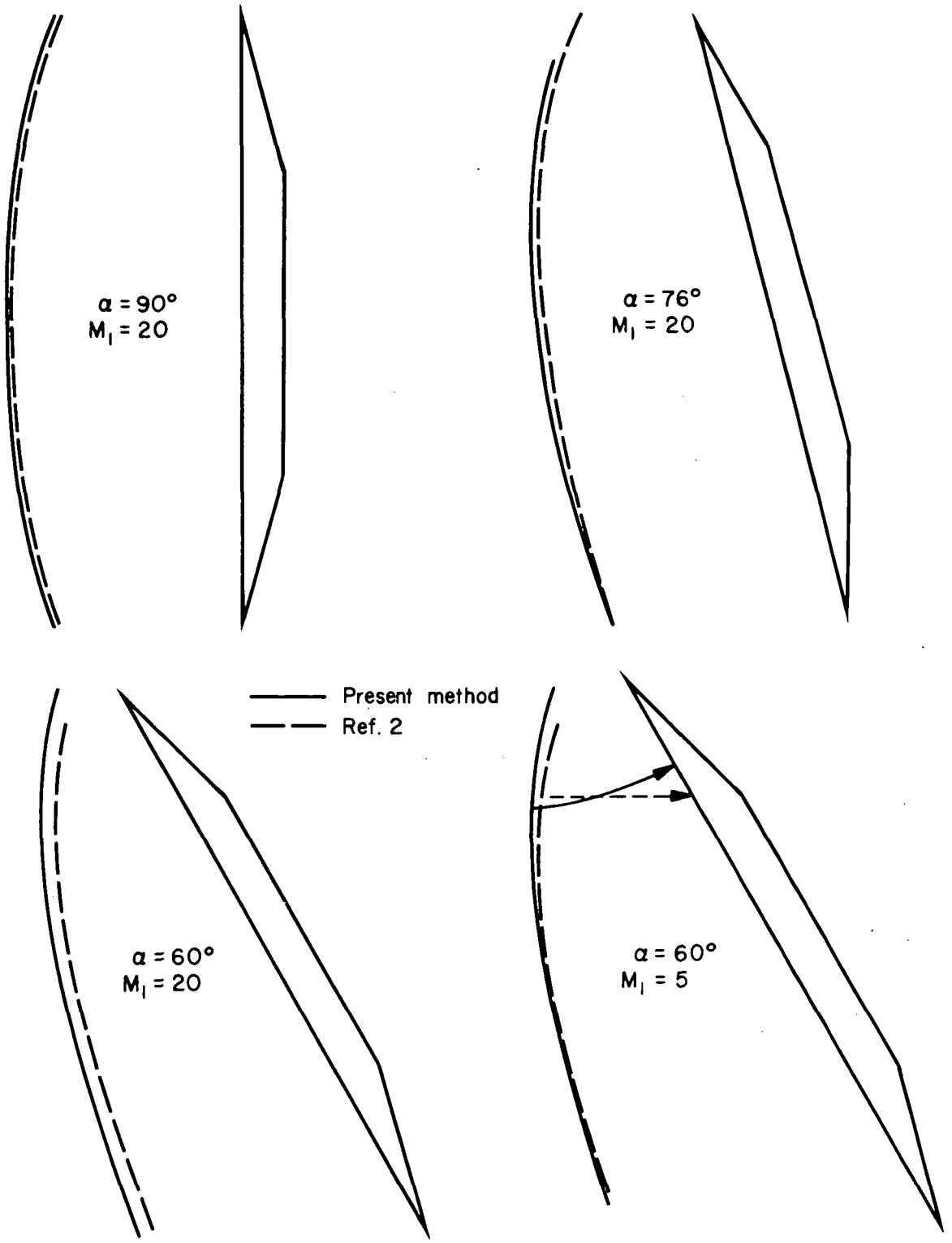

Figure 13.- Comparison of predicted shock on a two-dimensional plate of various angles of attack.

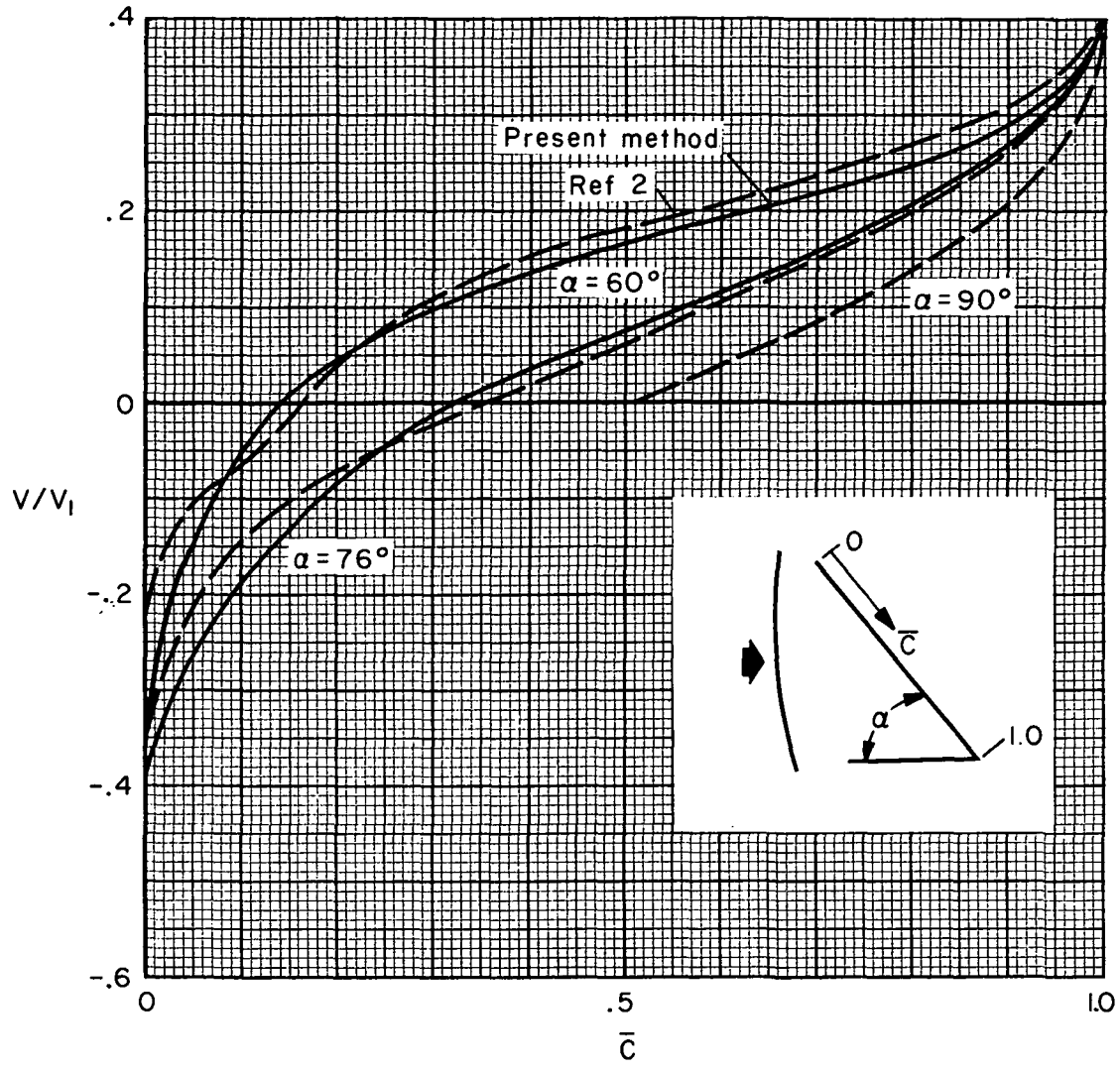

Figure 14.- Comparison of predicted velocity distribution on a two-dimensional plate of various angles of attack, $M_1 = 20$.

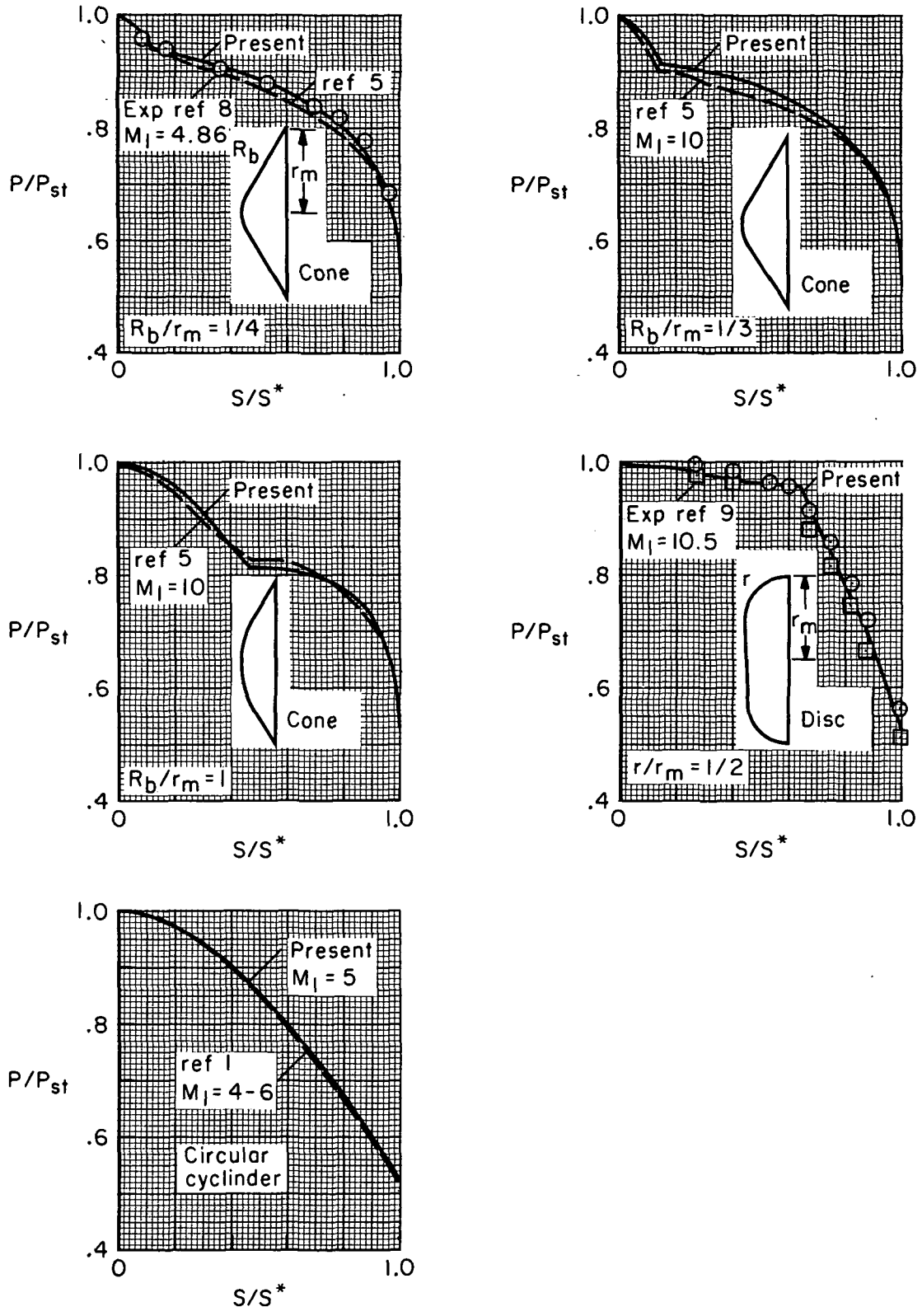

Figure 15.- Predicted and experimental pressure distributions on various bodies.

NATIONAL AERONAUTICS AND SPACE ADMINISTRATION
WASHINGTON, D.C. 20546

OFFICIAL BUSINESS
PENALTY FOR PRIVATE USE $300

SPECIAL FOURTH-CLASS RATE BOOK

POSTAGE AND FEES PAID
NATIONAL AERONAUTICS AND SPACE ADMINISTRATION
451

U.S.MAIL

POSTMASTER: If Undeliverable (Section 158 Postal Manual) Do Not Return

"The aeronautical and space activities of the United States shall be conducted so as to contribute . . . to the expansion of human knowledge of phenomena in the atmosphere and space. The Administration shall provide for the widest practicable and appropriate dissemination of information concerning its activities and the results thereof."

—NATIONAL AERONAUTICS AND SPACE ACT OF 1958

NASA SCIENTIFIC AND TECHNICAL PUBLICATIONS

TECHNICAL REPORTS: Scientific and technical information considered important, complete, and a lasting contribution to existing knowledge.

TECHNICAL NOTES: Information less broad in scope but nevertheless of importance as a contribution to existing knowledge.

TECHNICAL MEMORANDUMS: Information receiving limited distribution because of preliminary data, security classification, or other reasons. Also includes conference proceedings with either limited or unlimited distribution.

CONTRACTOR REPORTS: Scientific and technical information generated under a NASA contract or grant and considered an important contribution to existing knowledge.

TECHNICAL TRANSLATIONS: Information published in a foreign language considered to merit NASA distribution in English.

SPECIAL PUBLICATIONS: Information derived from or of value to NASA activities. Publications include final reports of major projects, monographs, data compilations, handbooks, sourcebooks, and special bibliographies.

TECHNOLOGY UTILIZATION PUBLICATIONS: Information on technology used by NASA that may be of particular interest in commercial and other non-aerospace applications. Publications include Tech Briefs, Technology Utilization Reports and Technology Surveys.

Details on the availability of these publications may be obtained from:

SCIENTIFIC AND TECHNICAL INFORMATION OFFICE

NATIONAL AERONAUTICS AND SPACE ADMINISTRATION

Washington, D.C. 20546